

Detection possibility of a Pseudo-FIMP in presence of a thermal WIMP

Subhaditya Bhattacharya,^a Jayita Lahiri,^b Dipankar Pradhan^a

^a*Department of Physics, Indian Institute of Technology Guwahati,
North Guwahati, Assam-781039, India,*

^b*II. Institut für Theoretische Physik, Universität Hamburg, 22761 Hamburg, Germany.*

E-mail: subhab@iitg.ac.in, jayita.lahiri@desy.de, d.pradhan@iitg.ac.in

ABSTRACT: A dark matter (DM) having feeble interaction with the visible sector can thermalise via substantial interaction with a Weakly Interacting Massive Particle (WIMP). Such DM candidates are categorised as pseudo-FIMP (pFIMP). pFIMP can provide both direct and indirect search prospects via WIMP loop. This work focuses into such possibilities. We provide all such one loop graphs involving scalar, fermion and vector boson particles via which pFIMP can interact with the Standard Model assuming both of them are stabilised via $\mathbb{Z}_2 \otimes \mathbb{Z}'_2$ symmetries. We elaborate upon a model where a fermion DM acts as WIMP and a scalar singlet acts as pFIMP having negligible Higgs portal interaction and substantial conversion via Yukawa interaction. We study in details the loop induced direct and indirect search prospects of the pFIMP in the relic density allowed region of the model.

KEYWORDS: Models for Dark Matter, Particle Nature of Dark Matter, Specific BSM Phenomenology.

Contents

1	Introduction	1
2	WIMP-pFIMP ensemble	3
2.1	A generic discussion	3
2.2	Possible pFIMP-WIMP interactions	5
3	Model example of a pFIMP-WIMP scenario	7
4	Dark matter phenomenology	9
4.1	Coupled Boltzmann Equations and Relic allowed parameter space	9
4.2	Direct detection prospect	13
4.2.1	Direct detection of WIMP	13
4.2.2	Direct detection of pFIMP	14
4.3	Indirect detection possibility	18
5	Conclusion	19
A	BEQ with Coannihilation of dark matter in Wimp-Fimp framework	20
B	Relevant Fermion Loop Calculations for direct search	21
C	Calculation of direct detection cross-section of pFIMP	26
D	Calculation of direct detection cross-section of WIMP	29
E	Higgs and Z Invisible decay width	30

1 Introduction

Particle dark matter (DM) has long been studied as it caters to most of the astrophysical and cosmological observations in a consistent manner. Apart from the electromagnetic charge neutrality and stability over the scale of universe's life time, there are not many unique characteristics that can be assigned to a DM particle. There exists a plethora of possibilities based on how it saturates the observed relic density as given by the PLANCK data ($\Omega_{\text{DM}}h^2 = 0.1200 \pm 0.0012$ [1]). In one class of models, the DM remains in equilibrium with thermal bath due to sizable interaction with the visible sector. Then it freezes out as the universe expands and cools down. If the depletion of DM occurs via $2_{\text{DM}} \rightarrow 2_{\text{SM}}$ interactions, then the annihilation cross-section required for the DM to attain correct relic density is of the order of electroweak interaction ($\sim 10^{-10} \text{ GeV}^{-2}$). Hence, such class of particles are dubbed as Weakly Interacting Massive Particle (WIMP) [2, 3]. In cases where

the number changing processes are governed mainly within the dark sector via $3_{\text{DM}} \rightarrow 2_{\text{DM}}$ or $4_{\text{DM}} \rightarrow 2_{\text{DM}}$ processes, the annihilation cross-section requires to be much higher to adjust the additional phase factor suppression and such class of DM particles are called Strongly Interacting Massive Particle (SIMP) [4]. The other possibility is to assume the DM having a feeble interaction with the visible sector, so that the DM remains out of equilibrium and gets produced via decay or annihilation of thermal bath particles and saturates when the temperature drops below the DM mass. Such particles are called Feebly Interacting Massive Particles (FIMP) [5]. Several other possibilities like SIDM [6, 7], cannibal DM [8], have also been ideated. Our discussion will mostly be centred around WIMP and FIMP.

Detectability of these different DM particles often provide the key distinctive features amongst them. WIMPs having sizeable interaction with the SM have been explored in direct DM search experiments via nuclear/electron recoil in XENON [9–11], PandaX [12, 13], LUX-ZEPLIN [14] etc although not found yet. Similar signal for FIMP or SIMP is often difficult just because of the small interaction cross-section. Apart from the direct search, collider search of DM has been extensively studied where the DM carries away missing momentum or energy in presence of some visible leptons, photons or jets, both in context of LHC [15–23] and ILC [24–30]. Again, WIMPs have the best bet to provide such signals [3, 31], while for FIMP one has to look for disappearing charge track or displaced vertex signal, see for example, [32]. However, null observation in both direct and collider searches put bounds on the available parameter space. Apart from these terrestrial DM search experiments, indirect search for DM stemming from its annihilation into photon [33–35], anti-proton [36–39] or positron [40–42] via their excess fluxes in the centre of galaxies have been studied. Again, FIMP type models are difficult to probe in such cases as well.

Dark sector constituting of more than one DM components is the focus of the current paper. Two-component DM models have been proposed in various cases [43–46] and extensively studied in many [47–49]. They provide many new features, the pivotal point of which encompass around the issue of DM-DM interaction or conversion. WIMP-WIMP models show features like modified freeze-out and modified direct search prospects [46]. Two component FIMP models have recently been studied where the interaction can cater to structure formation issues [50]. WIMP-FIMP interaction on the other hand, when feeble, helps FIMP production from the WIMP, but doesn't have too much phenomenological advantage. However, when WIMP-FIMP interaction is of the weak interaction strength, it brings the FIMP to thermal bath, as proposed recently [51], called pseudo-FIMP or pFIMP. pFIMPs always rely on the conversion for the freeze-out and this makes them distinct from their WIMP partner. pFIMP possibilities have been explored in literature [46–48], but without detailing upon its potential characteristics or phenomenological consequences.

We study a model with two DM components, a scalar and a fermion. The minimal version of such a framework has already been discussed in [46], where the fermion DM acts as pFIMP, while the scalar acts as WIMP. However, the allowed parameter space turns very constrained. We rather choose the scalar DM to be pFIMP, while the fermion sector is enlarged with a vector like doublet and a singlet, where the lightest one after mixing via electroweak symmetry breaking (EWSB) serves as the WIMP component having gauge interaction with the visible sector. One of the most interesting aspects of pFIMP is the

possibility of bringing them under direct search scanner via WIMP loop, which is the highlight of this paper. The possibilities in indirect search experiments have also been discussed.

The paper is organised as follows. In Section 2, we present a general discussion on the WIMP-pFIMP scenario and possible interactions between WIMP and pFIMP, that can give rise to interesting prospects in detection experiments. In Section 3, we propose a model constituting two-component DM, that can give rise to WIMP-pFIMP. The dark matter phenomenology of this model including the its relic density and prospect of direct and indirect detection are discussed in detail in Section 4. In Section 5, we summarize our discussion and conclude.

2 WIMP-pFIMP ensemble

We have demonstrated in [51], that a FIMP like DM can thermalise via sizable interaction with an WIMP, when it is called a pFIMP. Importantly, most of the pFIMP characteristics can be described in a model independent way. In the following, we will have a short account of it before going into different possible frameworks where pFIMP can be realised.

2.1 A generic discussion

The freeze-out pattern of pFIMP is governed via a generic coupled Boltzmann Equations (cBEQ) as given by,

$$\begin{aligned}
\frac{dY_1}{dx} &= -\frac{2\pi^2 M_{\text{pl}}}{45 \times 1.67} \frac{g_\star^s}{\sqrt{g_\star^p}} \frac{\mu_{12}}{x^2} \left[\langle \sigma v \rangle_{11 \rightarrow \text{SM}} \left(Y_1^2 - Y_1^{\text{eq}^2} \right) \right. \\
&\quad \left. + \langle \sigma v \rangle_{11 \rightarrow 22} \left(Y_1^2 - \frac{Y_1^{\text{eq}^2}}{Y_2^{\text{eq}^2}} Y_2^2 \right) \right], \\
\frac{dY_2}{dx} &= \frac{2M_{\text{pl}}}{1.67 \times \sqrt{g_\star^p}} \frac{x}{\mu_{12}^2} \langle \Gamma_{\text{SM} \rightarrow 22} \rangle (Y_{\text{SM}}^{\text{eq}} - \frac{Y_2^2}{Y_2^{\text{eq}^2}} Y_{\text{SM}}^{\text{eq}}) \\
&\quad + \frac{4\pi^2 M_{\text{pl}}}{45 \times 1.67} \frac{g_\star^s}{\sqrt{g_\star^p}} \frac{\mu_{12}}{x^2} \left[\langle \sigma v \rangle_{\text{SM} \rightarrow 22} \left(Y_{\text{SM}}^{\text{eq}^2} - \frac{Y_2^2}{Y_2^{\text{eq}^2}} Y_{\text{SM}}^{\text{eq}^2} \right) \right. \\
&\quad \left. + \langle \sigma v \rangle_{11 \rightarrow 22} \left(Y_1^2 - \frac{Y_1^{\text{eq}^2}}{Y_2^{\text{eq}^2}} Y_2^2 \right) \right].
\end{aligned} \tag{2.1}$$

In the above and also in the rest of the draft, subscripts 1, 2 denote WIMP and FIMP (pFIMP) components respectively. The interaction channels which crucially govern the freeze-out/freeze-in of the DM components are:

- $\text{DM}_1, \text{DM}_1 \rightarrow \text{SM}, \text{SM}$: annihilation/depletion of the WIMP to the SM states, denoted by $\langle \sigma v \rangle_{11 \rightarrow \text{SM}}$,
- $\text{DM}_1, \text{DM}_1 \rightarrow \text{DM}_2, \text{DM}_2$: conversion of the WIMP to the FIMP (pFIMP) or vice versa, denoted by $\langle \sigma v \rangle_{11 \rightarrow 22}$,

- SM, SM \rightarrow DM₂, DM₂: production of the FIMP (pFIMP) from the thermal (SM) bath denoted by $\langle\sigma v\rangle_{\text{SM}\rightarrow 22}$,
- SM \rightarrow DM₂, DM₂: decay of the bath particles to the FIMP (pFIMP), denoted by $\langle\Gamma_{\text{SM}\rightarrow 22}\rangle$.

We note here that the cBEQ for a two component WIMP case is no different than WIMP-FIMP case as shown in Eq. 2.1. The difference lies in the strength of the DM-SM interactions ($\langle\sigma v\rangle_{\text{WIMP}} \sim 10^{-8} \text{ GeV}^{-2}$, whereas $\langle\sigma v\rangle_{\text{FIMP}} \sim 10^{-20} \text{ GeV}^{-2}$). The other difference lies in the initial conditions on yield, for WIMP: $Y_1|_{x\sim 0} = Y_1^{\text{eq}} \sim x^{3/2}e^{-x}$, while for FIMP: $Y_2|_{x\sim 0} = 0$. The pFIMP solution is obtained when

$$\text{pFIMP} : \langle\sigma v\rangle_{\text{SM}\rightarrow 22}, \langle\Gamma_{\text{SM}\rightarrow 22}\rangle \ll \langle\sigma v\rangle_{11\rightarrow 22} \sim \langle\sigma v\rangle_{11\rightarrow \text{SM}} \sim 10^{-12} \text{ GeV}^{-2}. \quad (2.2)$$

The pFIMP becomes WIMP when $\langle\sigma v\rangle_{\text{SM}\rightarrow 22}, \langle\Gamma_{\text{SM}\rightarrow 22}\rangle \sim \langle\sigma v\rangle_{11\rightarrow 22} \sim \langle\sigma v\rangle_{11\rightarrow \text{SM}}$. We further note that the cBEQ is written in terms of yields $Y_{1,2} = \frac{n_{1,2}}{s}$, where s refers to the entropy density (per co-moving volume) as,

$$s = \frac{2\pi^2}{45} g_\star^s(T) T^3; \quad g_\star^s(T) = \sum_k \mathcal{C}_k g_k \left(\frac{T_k}{T}\right)^3 \theta(T - m_k). \quad (2.3)$$

Here k runs over all particles, T_k is the temperature of particle k , g_k its number of internal degrees of freedom and $\mathcal{C}_k = 1$ (7/8) when k is a boson(fermion). We also define the Hubble parameter as

$$\mathcal{H}(T) = 1.67 \sqrt{g_\star^p} \frac{T^2}{M_{\text{pl}}}; \quad g_\star^p(T) = \sum_{i=\text{bosons}} g_i \left(\frac{T_i}{T}\right)^4 + \frac{7}{8} \sum_{i=\text{fermions}} g_i \left(\frac{T_i}{T}\right)^4. \quad (2.4)$$

We will assume the relativistic degrees of freedom (DOF) $g_\star^{\rho,s} \approx 106.7$ to be approximately constant as the temperature during which the FIMP freezes in or the WIMP freezes out is rather high. Note that, since two DM with different masses $m_{1,2}$ are involved, we define a common variable $x = \mu_{12}/T$ where $\mu_{12} = m_1 m_2 / (m_1 + m_2)$ is the reduced mass of the system of two DMs. This is possible in particular to the pFIMP solution, when both pFIMP and WIMP share the same temperature. With the redefined x we can write the equilibrium yield [2] as,

$$Y_i^{\text{eq}}(x) = \frac{45}{4\pi^4} \frac{g_i}{g_\star^s} \left(\frac{m_i}{\mu_{12}} x\right)^2 K_2\left(\frac{m_i}{\mu_{12}} x\right). \quad (2.5)$$

The expressions of thermal average of annihilation cross-section is given by,

$$\langle\sigma v\rangle = \frac{1}{8m^4 T} \frac{1}{K_2(m/T)^2} \int_{4m^2}^{\infty} \sigma(s) (s - 4m^2) \sqrt{s} K_1\left(\frac{\sqrt{s}}{T}\right) ds, \quad (2.6)$$

where $v = 1/(E_1 E_2) (\sqrt{(p_1 \cdot p_2)^2 - m_1^2 m_2^2})$ denotes Mollar velocity, s denotes center-of-mass (c.o.m) energy and m denotes DM mass. We further note that the conversion from one DM species to the other are related by:

$$\langle\sigma v\rangle_{11\rightarrow 22} = \langle\sigma v\rangle_{22\rightarrow 11} \left(\frac{Y_2^{\text{eq}}}{Y_1^{\text{eq}}}\right)^2. \quad (2.7)$$

The above relation basically indicates that, when WIMP is heavier than pFIMP, i.e. $m_1 > m_2$ (hierarchy 1), the conversion from WIMP to pFIMP is kinematically allowed, while the reverse process is Boltzmann suppressed by a factor $\sim e^{-2x\delta m}$, where δm is the mass difference between the two DM's. The converse is true when pFIMP is heavier than WIMP, i.e. $m_2 > m_1$ (hierarchy 2). This plays an important role to distinguish the allowed parameter space of the pFIMP-WIMP case for different mass hierarchies. The key features of pFIMP freeze out are discussed in details in [51], a summary of which is as follows:

- pFIMP freezes out together or before WIMP, so the relic density of pFIMP is always larger than the WIMP partner¹. When the conversion cross-section is of similar order to that of WIMP annihilation to SM, both pFIMP and WIMP share similar relic densities.
- When the conversion rate is higher than the WIMP annihilation, the freeze out and resultant relic density of pFIMP remains constant in hierarchy 1, while the WIMP relic becomes much smaller. In hierarchy 2, this is exactly the other way round. With larger conversion, the WIMP relic remains constant and pFIMP relic drops sharply.
- The mass splitting between WIMP and pFIMP needs to be small for the relic density and direct search allowed parameter space, with $\delta m \sim 10$ GeV, for ~ 100 GeV WIMP or pFIMP.

2.2 Possible pFIMP-WIMP interactions

pFIMPs do not have a sizeable interaction with the SM particles, but thanks to the interaction with WIMPs, they can have a one loop interaction to SM. We first discuss the possible scenarios in a model-independent manner under which a pFIMP can interact with SM states and thereby can produce DM signal at the future direct and indirect search experiments. Possible pFIMP-SM interactions via WIMP loop are shown in Figure 1. Here WIMPs are denoted by red lines, pFIMPs by black lines and the WIMP portals (Z/h or heavy NP particles) with SM by grey lines. The dashed, solid and wavy lines indicate scalar, fermion and vector bosons. While drawing these vertices, we have kept the spin conservation in mind. Also, pFIMPs and WIMPs are expected to be stabilized under separate symmetries. Therefore, the particles denoted by teal color lines are expected to transform suitably under both the symmetries.

In Table 1, we have shown possible renormalizable interactions between WIMP and pFIMP in two component DM scenarios stabilized by $\mathbb{Z}_2 \otimes \mathbb{Z}'_2$ for all combinations of scalar, fermion and vector boson particles. The scenarios have one to one correspondence to the vertices shown in Fig. 1. WIMPs are odd under \mathbb{Z}_2 and even under \mathbb{Z}'_2 , while pFIMPs are odd under \mathbb{Z}'_2 , and even under \mathbb{Z}_2 . Note that particles denoted by prime like $(\chi', \psi', \phi', X'_\mu)$, charged under both $\mathbb{Z}_2 \otimes \mathbb{Z}'_2$, connect WIMP and pFIMP states, as shown by teal color lines in Fig.1. This list excludes dark sector particles having non-trivial SM charges and SM particles having dark charges as well as more complicated spin configurations and higher order operators having mass dimension larger than four. The right and cross signs in the

¹Recall that $\Omega_{\text{WIMP}} h^2 \sim 1/\langle\sigma v\rangle$.

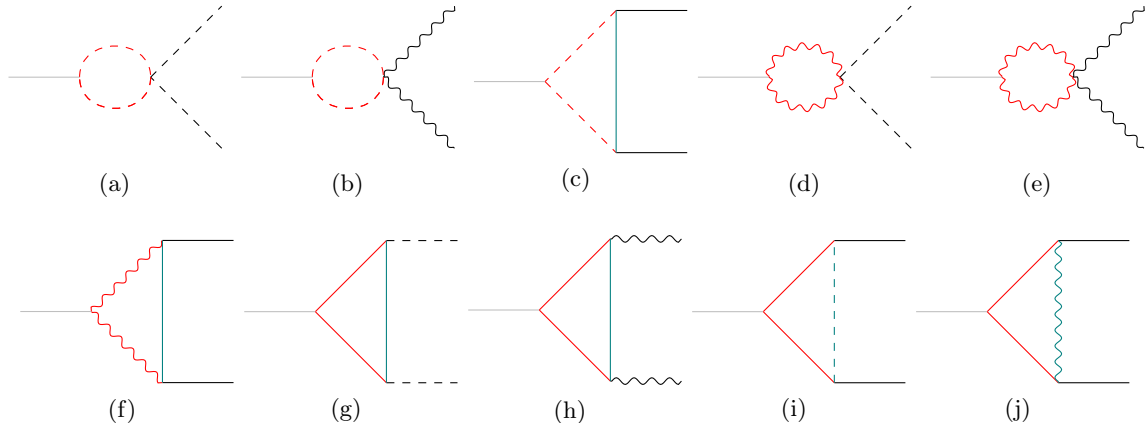


Figure 1: Sample Feynman diagrams showing pFIMP interaction with SM via WIMP loops where WIMP, pFIMP, SM ($h/Z/\gamma$) and a heavy thermal bath particle are represented by red, black, grey and teal color lines respectively. All possible combinations of scalar (dashed), fermion (solid) and vector boson (wavy lines) particles are shown assuming the WIMP and pFIMP to transform under different stabilizing symmetries.

Scenarios	Two component DM Model			Relic	Detection Possibility
	WIMP	pFIMP	WIMP-pFIMP Interaction		
(a)	Scalar(ϕ)	Scalar(Φ)	$\phi^2\Phi^2$	✓[47, 51]	✗
(b)	Scalar(ϕ)	Vector(V)	$\phi^2V^\mu V_\mu$	✗	✗
(c)	Scalar(ϕ)	Fermion(χ)	$\bar{\chi}\chi'\phi$	✓[46]	✓[46]
(d)	Vector(X)	Scalar(Φ)	$X^\mu X_\mu\Phi^2$	✗	✗
(e)	Vector(X)	Vector(V)	$X^\mu X_\mu V^\nu V_\nu$	✗	✗
(f)	Vector(X)	Fermion(χ)	$\bar{\chi}\gamma^\mu\chi'X_\mu$	✗	✗
(g)	Fermion(ψ)	Scalar(Φ)	$\bar{\psi}\psi'\Phi$	This work	This work
(h)	Fermion(ψ)	Vector(V)	$\bar{\psi}\gamma^\mu\psi'V_\mu$	✗	✗
(i,j)	Fermion(ψ)	Fermion(χ)	$\bar{\psi}\chi\phi', \bar{\psi}\gamma^\mu\chi X'_\mu$	✓[48]	✗

Table 1: The possible two-component WIMP-pFIMP set-ups (respective Feynman diagrams in Fig.1). Prime particles ($\chi', \psi', \phi', X'_\mu$) are \mathbb{Z}_2 – odd and \mathbb{Z}'_2 – odd bath particles connecting both WIMP-pFIMP.

relic and detection possibilities in Table 1 indicate whether such possibilities have been studied before or not. A short account of these models and their interactions are as follows:

- (i) Figures 1a, 1b, 1d and 1e correspond to two-component scalar-scalar, scalar-vector, vector-scalar, vector-vector DM scenarios. In these class of models, WIMPs and pFIMPs are connected without a third particle.
- (ii) Figure 1c and 1f correspond to two-component DM set up, where the WIMP are scalar or vector-boson while pFIMP is a Dirac-fermion, connected by another thermal bath fermion odd under both \mathbb{Z}_2 , and \mathbb{Z}'_2 .
- (iii) Figure 1g and 1h denote a scenario where WIMP is a Dirac fermion and pFIMPs are scalar or vector-boson particles, again connected by a thermal bath fermionic particle odd under both \mathbb{Z}_2 , and \mathbb{Z}'_2 .
- (iv) Finally, Figures 1i and 1j correspond to a situation where both WIMP and pFIMPs are fermions connected by a scalar (Fig. 1i) or a vector-boson (Fig. 1j) particle, odd under both \mathbb{Z}_2 , and \mathbb{Z}'_2 .

3 Model example of a pFIMP-WIMP scenario

Amongst the possibilities described in Table 1, the WIMP-pFIMP phenomenology has been explored in the case of two-component scalar DM model [47, 51]. It has been pointed out that when pFIMP couples to the SM states via a scalar WIMP loop, it is not possible to achieve a relic density allowed parameter space where the scalar pFIMP can be detected in future direct detection experiment. We will elaborate more on this later. In [46], the direct detection prospect of a fermion pFIMP was studied in a scalar-fermion set up as in Fig. 1c, without elaborating upon the pFIMP characteristics. The resulting parameter space of this model is highly constrained by the recent most direct search results. In [48], pFIMP phenomenon was discussed partially, but detectability of pFIMP via WIMP loop has been neglected. We will focus on a WIMP-pFIMP set up where the direct detection possibility of pFIMP is achieved in next generation experiment and make connections with indirect detection as well. Unlike the model-independent approach taken in [51], here we elaborate on the channels through which the freeze-out can occur for both the DM components taking temperature-dependence of all the annihilation cross-sections and decay widths into consideration.

Our model consists of (i) a real scalar-singlet DM ϕ , which acts like pFIMP and (ii) the lightest admixture of a vector-like fermion doublet $\psi = (\psi^0 \ \psi^-)^T$ [52] and a vector-like singlet fermion ψ_1 , which behaves like WIMP. We additionally introduce another vector-like singlet fermion ψ_2 , which acts as a messenger between the two DM sectors. Stability of both DM components can be ensured by a $\mathbb{Z}_2 \otimes \mathbb{Z}'_2$ symmetry. The quantum numbers of all the relevant fields are given in Table 2.

The corresponding Lagrangian can be written as;

$$\mathcal{L} \supset \mathcal{L}_{\text{Scalar}} + \mathcal{L}_{\text{VF}} , \tag{3.1}$$

Dark Fields	$SU(3)_c \times SU(2)_L \times U(1)_Y \times \mathbb{Z}_2 \times \mathbb{Z}'_2$				
$\psi = \begin{pmatrix} \psi^0 \\ \psi^- \end{pmatrix}$	1	2	-1	-	+
ψ_1	1	1	0	-	+
ψ_2	1	1	0	+	-
ϕ	1	1	0	-	-

Table 2: Dark sector fields and their corresponding quantum numbers.

where,

$$\mathcal{L}_{\text{Scalar}} = \frac{1}{2} |\partial_\mu \phi|^2 - \frac{1}{2} \mathbf{m}_\phi^2 \phi^2 - \frac{1}{4!} \lambda_\phi \phi^4 - \frac{1}{2} \lambda_{\phi H} \phi^2 H^\dagger H, \quad (3.2)$$

$$\begin{aligned} \mathcal{L}_{\text{VF}} = & \bar{\psi} \left[i\gamma^\mu \left(\partial_\mu + ig \frac{\sigma^a}{2} W_\mu^a + ig' \frac{Y}{2} B_\mu \right) - m_\psi \right] \psi + \sum_{\alpha=1,2} \bar{\psi}_\alpha (i\gamma^\mu \partial_\mu - m_{\psi_\alpha}) \psi_\alpha \\ & - (Y_1 \bar{\psi} \tilde{H} \psi_1 + Y_2 \bar{\psi}_2 \psi_1 \phi + \text{h.c.}) ; \end{aligned} \quad (3.3)$$

After Electroweak Symmetry Breaking(EWSB), SM Higgs H acquires vacuum expectation value(VEV) ($v = 246$ GeV) and in unitarity gauge we can write, $H = \left(0 \quad \frac{1}{\sqrt{2}}(v+h) \right)^T$. After symmetry breaking the physical mass term of ϕ can be written as $m_\phi^2 = \mathbf{m}_\phi^2 + \frac{1}{2} \lambda_{\phi H} v^2$. ϕ is a stable DM candidate and serves as pFIMP with negligible $\lambda_{\phi H}$. From Eq.3.3, it is straight-forward to calculate the mass terms for the vector-like fermions. The mass eigenstates (χ_1, χ_2) can be obtained via diagonalization of the fermion mass matrix through a unitary transformation from the flavour basis (ψ_1, ψ^0).

$$-\mathcal{L}_{\text{mass}} = m_{\chi_1} \bar{\chi}_1 \chi_1 + m_{\chi_2} \bar{\chi}_2 \chi_2 + m_\psi \psi^+ \psi^- ; \quad (3.4)$$

where,

$$\begin{aligned} \chi_1 &= \cos \theta \psi_1 + \sin \theta \psi^0, \\ \chi_2 &= -\sin \theta \psi_1 + \cos \theta \psi^0, \\ m_{\chi_1} &= \sin^2 \theta m_\psi + \cos^2 \theta m_{\psi_1} + \frac{Y_1 v}{\sqrt{2}} \sin 2\theta, \\ m_{\chi_2} &= \cos^2 \theta m_\psi + \sin^2 \theta m_{\psi_1} - \frac{Y_1 v}{\sqrt{2}} \sin 2\theta. \end{aligned} \quad (3.5)$$

The mixing angle θ can be written as,

$$\tan 2\theta = \frac{\sqrt{2} Y_1 v}{m_{\psi_1} - m_\psi}. \quad (3.6)$$

Using Eq. 3.6, we can easily write,

$$Y_1 = \frac{\sin 2\theta}{\sqrt{2}v} (m_{\chi_1} - m_{\chi_2}), \quad (3.7)$$

$$m_\psi = m_{\chi_1} \sin^2 \theta + m_{\chi_2} \cos^2 \theta, \quad (3.8)$$

$$m_{\psi_1} = m_{\chi_1} \cos^2 \theta + m_{\chi_2} \sin^2 \theta. \quad (3.9)$$

m_ψ denotes the mass of the charged component of vector like fermion doublet ψ^\pm . The independent parameters of our model are $\{m_{\chi_1}, m_{\chi_2}, m_{\psi_2}, m_\phi, \sin\theta, Y_2, \lambda_{\phi H}\}$. χ_1 being the lightest neutral fermion, serves as the WIMP DM and the mass difference between χ_1 and the second lightest neutral fermion χ_2 is denoted as $\Delta m = m_{\chi_2} - m_{\chi_1}$. Mass difference between χ_1 and ϕ is denoted by $\delta m = m_\phi - m_{\chi_1}$ and serves as an important parameter in the WIMP-pFIMP set up.

The interaction between WIMP and pFIMP occurs via the Yukawa term, $Y_2 \bar{\psi}_1 \psi_2 \phi$, which is crucial for the WIMP-pFIMP conversion. We will be particularly interested in the region where $m_{\psi_2} > m_{\chi_1} + m_\phi$, so that ψ_2 can decay into χ_1 and ϕ . The relevant Feynman diagrams for pFIMP production, (co)-annihilation of WIMPs and WIMP-pFIMP conversions are shown in Figures. 2, 3 and 4. We would like to further mention that a tiny $\lambda_{\phi H} \sim 10^{-10}$ as required for pFIMP realisation, helps evading the upper bound on Higgs invisible branching ratio $\text{BR}(h \rightarrow \text{invisible}) < 19\%$ at 2σ [53] as well as the direct detection constraints. It allows us to explore the mass range below the Higgs resonance $m_\phi < (m_h/2)$. We would like to mention, we have checked the constraints from limits on Higgs and Z invisible decay width (see Appendix E, when DM masses are below such resonances).

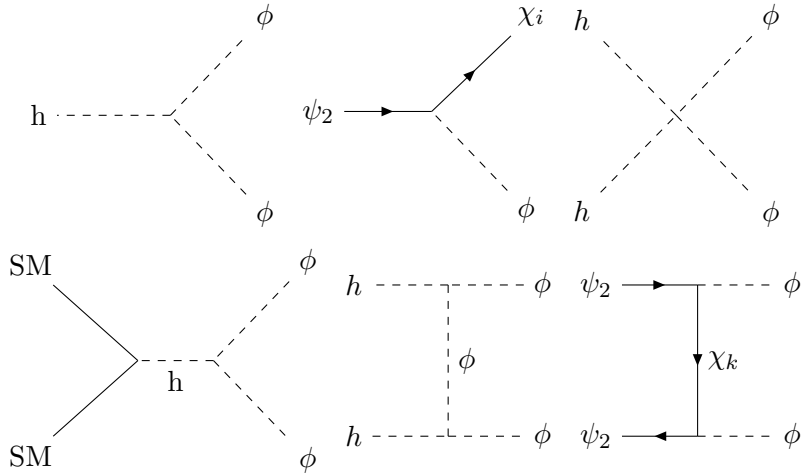


Figure 2: Feynman diagrams for pFIMP ϕ production from thermal bath ($\{i, k = 1, 2\}$).

4 Dark matter phenomenology

Having discussed the model, we will focus on the DM phenomenology highlighting the pFIMP behaviour.

4.1 Coupled Boltzmann Equations and Relic allowed parameter space

We begin with the cBEQ's, specific to our model after considering all the relevant processes [54–58],

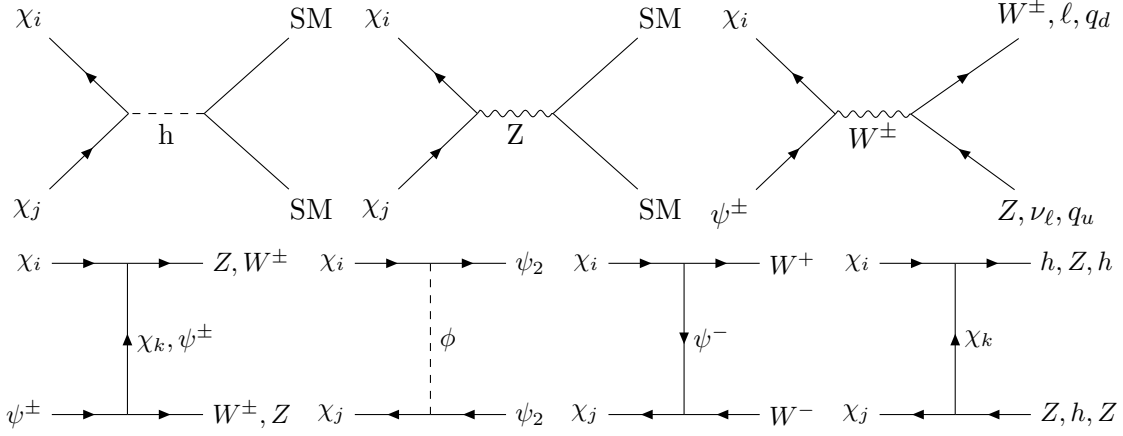


Figure 3: Feynman diagrams for the possible annihilation and co-annihilation channels of WIMP χ_1 ($\{i, j, k = 1, 2\}$).

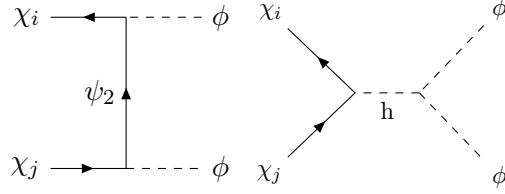


Figure 4: Feynman diagrams contributing to WIMP-pFIMP conversion ($\{i, j = 1, 2\}$).

$$\begin{aligned}
\frac{dY_\chi}{dx} = & -\frac{2\pi^2 M_{\text{pl}}}{45 \times 1.67} \frac{g_\star^s}{\sqrt{g_\star^\rho}} \frac{\mu_{\chi_1 \phi}}{x^2} \left[\langle \sigma v \rangle_{\text{SM}}^{\text{eff}} (Y_\chi^2 - Y_\chi^{\text{eq}^2}) + \langle \sigma v \rangle_\phi^{\text{eff}} \left(Y_\chi^2 - Y_\chi^{\text{eq}^2} \frac{Y_\phi^2}{Y_\phi^{\text{eq}^2}} \right) \right. \\
& - \langle \sigma v \rangle_{\psi_2}^{\text{eff}} \left(Y_\chi^2 - Y_\chi^{\text{eq}^2} \frac{Y_{\psi_2}^2}{Y_{\psi_2}^{\text{eq}^2}} \right) + \langle \sigma v \rangle_{\chi_1 \bar{\psi}_2 \rightarrow h \phi}^{\text{eff}} \left(Y_{\psi_2} Y_\chi - Y_{\psi_2}^{\text{eq}} Y_\chi^{\text{eq}} \frac{Y_\phi}{Y_\phi^{\text{eq}}} \right) \left. \right] \quad (4.1) \\
& + \frac{M_{\text{pl}}}{1.67 \sqrt{g_\star^\rho}} \frac{x}{\mu_{\chi_1 \phi}^2} \langle \Gamma \rangle_{\psi_2 \rightarrow \chi_1 \phi}^{\text{eff}} \left(Y_{\psi_2} - Y_{\psi_2}^{\text{eq}} \frac{Y_\phi}{Y_\phi^{\text{eq}}} \frac{Y_\chi}{Y_\chi^{\text{eq}}} \right),
\end{aligned}$$

$$\begin{aligned}
\frac{dY_\phi}{dx} = & \frac{M_{\text{pl}}}{1.67 \times \sqrt{g_\star^\rho}} \frac{x}{\mu_{\chi_1 \phi}^2} \left[2 \langle \Gamma \rangle_{h \rightarrow \phi \phi} \left(Y_h^{\text{eq}} - Y_h^{\text{eq}} \frac{Y_\phi^2}{Y_\phi^{\text{eq}^2}} \right) + \langle \Gamma \rangle_{\psi_2 \rightarrow \chi_1 \phi}^{\text{eff}} \left(Y_{\psi_2} - Y_{\psi_2}^{\text{eq}} \frac{Y_\phi}{Y_\phi^{\text{eq}}} \frac{Y_\chi}{Y_\chi^{\text{eq}}} \right) \right] \\
& + \frac{2\pi^2 M_{\text{pl}}}{45 \times 1.67} \frac{g_\star^s}{\sqrt{g_\star^\rho}} \frac{\mu_{\chi_1 \phi}}{x^2} \left[2 \langle \sigma v \rangle_{\text{SM SM} \rightarrow \phi \phi} \left(Y_{\text{SM}}^{\text{eq}^2} - Y_{\text{SM}}^{\text{eq}^2} \frac{Y_\phi^2}{Y_\phi^{\text{eq}^2}} \right) \right. \\
& + 2 \langle \sigma v \rangle_{\psi_2 \bar{\psi}_2 \rightarrow \phi \phi} \left(Y_{\psi_2}^2 - Y_{\psi_2}^{\text{eq}^2} \frac{Y_\phi^2}{Y_\phi^{\text{eq}^2}} \right) + \langle \sigma v \rangle_{\chi_1 \bar{\psi}_2 \rightarrow h \phi}^{\text{eff}} \left(Y_{\psi_2} Y_\chi - Y_{\psi_2}^{\text{eq}} Y_\chi^{\text{eq}} \frac{Y_\phi}{Y_\phi^{\text{eq}}} \right) \\
& \left. + 2 \langle \sigma v \rangle_\phi^{\text{eff}} \left(Y_\chi^2 - Y_\chi^{\text{eq}^2} \frac{Y_\phi^2}{Y_\phi^{\text{eq}^2}} \right) \right]. \quad (4.2)
\end{aligned}$$

Eq. 4.1, and 4.2, are the cBEQ's of the WIMP(χ_1) and pFIMP(ϕ) respectively. In Eq. 4.1, Y_χ is the total WIMP DM yield and Y_ϕ is the pFIMP yield, the two crucial quantities for our analysis. In writing the Equations, we have used the following ansatz [54],

$$\frac{n_i}{n} \approx \frac{n_i^{\text{eq}}}{n^{\text{eq}}}, \quad (4.3)$$

where

$$n^{\text{eq}} = \sum_i n_i^{\text{eq}} = \frac{T}{2\pi^2} \sum_i g_i m_i^2 K_2\left(\frac{m_i}{T}\right). \quad (4.4)$$

We would like to mention, since in our model, we have an extended dark sector, where over and above the stable DM states χ_1 and ϕ , all the unstable heavy states such as ψ^\pm , χ_2 will also take part in co-annihilation as well as decay processes when in equilibrium. After freeze-out they will eventually decay into the stable lightest particle of the spectrum, namely χ_1 . In order take this effect in account, we have considered the 'effective' thermal average $\langle\sigma v\rangle^{\text{eff}}$ of annihilation cross-section and decay width $\langle\Gamma\rangle^{\text{eff}}$, see [59] and Appendix A for details. We emphasize that the total WIMP yield Y_χ will be the sum of the yields of all the particles which transform under the same Z_2 symmetry as χ_1 ,

$$Y_\chi = \sum_i Y_{\chi_i}, \quad \chi_i = \{\chi_1, \bar{\chi}_1, \chi_2, \bar{\chi}_2, \psi^\pm\}. \quad (4.5)$$

The SM final states in Eq. 4.1 and 4.2 includes all possible final states such as h, W^\pm, Z, ℓ, q . The common variable $x = \frac{\mu_{\chi_1\phi}}{T}$ written in terms of the reduced mass $\mu_{\chi_1\phi} = \left(\frac{1}{m_{\chi_1}} + \frac{1}{m_\phi}\right)^{-1}$ caters to the two component DM system. A symmetry factor of 2 applies in case of the scalar DM ϕ (see Eq. 4.2). The dark sector particles follow the non-relativistic equilibrium distribution given by,

$$Y_\chi^{\text{eq}} = \frac{45}{4\pi^4} \sum_i \frac{g_i}{g_\star^s} \left(x \frac{m_i}{\mu_{\chi_1\phi}}\right)^2 K_2\left(x \frac{m_i}{\mu_{\chi_1\phi}}\right), \quad (4.6)$$

$$Y_\phi^{\text{eq}} = \frac{45}{4\pi^4} \frac{g_\phi}{g_\star^s} \left(x \frac{m_\phi}{\mu_{\chi_1\phi}}\right)^2 K_2\left(x \frac{m_\phi}{\mu_{\chi_1\phi}}\right). \quad (4.7)$$

In the above equation, $M_{\text{pl}} = 1.22091 \times 10^{19}$ GeV and $g_\star^s \simeq g_\star^l \approx 106.7$. We have assumed that in our model χ_i, ψ^\pm are in equilibrium by rapid annihilations into bath particles. ψ_2 will also remain in equilibrium by virtue of the sizeable Y_2 , and we can assume $Y_{\psi_2} \approx Y_{\psi_2}^{\text{eq}}$ and neglect the evolution of ψ_2 separately. The scalar DM ϕ is assumed out-of-equilibrium initially, due to its tiny coupling with the SM particles, while ϕ reaches thermal equilibrium and becomes pFIMP, aided by large conversion between $\chi\chi \rightarrow \phi\phi$ mediated by ψ_2 , when Y_2 is large. Subsequent solution of the cBEQ provides relic density of the DM species by the following formula,

$$\Omega_{\text{DM}} h^2 = 2.74385 \times 10^8 \left(m_{\chi_1} Y_\chi \left[\frac{m_{\chi_1}}{\mu_{\chi_1\phi}} x_\infty \right] + m_\phi Y_\phi \left[\frac{m_\phi}{\mu_{\chi_1\phi}} x_\infty \right] \right), \quad (4.8)$$

where x_∞ corresponds to the present time. The solutions of cBEQ's are presented in terms

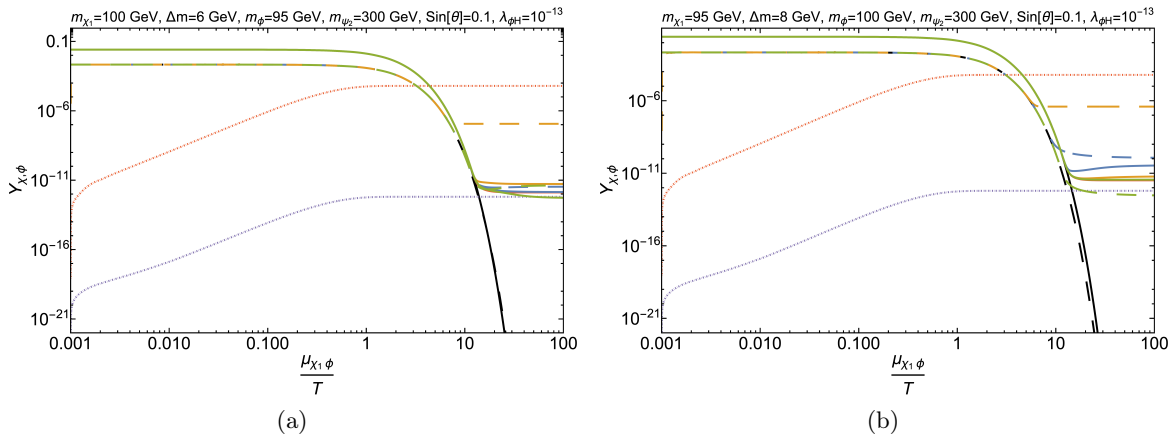


Figure 5: Figure 5(a) shows the variation of yield (Y) of WIMP (thick lines), pure FIMP (dotted lines) and pFIMP (dashed lines) as a function of x where violet, red, yellow, blue and green lines correspond to different values of Y_2 $\{10^{-12}, 10^{-8}, 10^{-2}, 1, 2\}$ respectively for $m_{\chi_1} > m_{\phi}$. Figure 5(b) shows the same for $m_{\chi_1} < m_{\phi}$ with different values of Yukawa coupling Y_2 $\{10^{-12}, 10^{-8}, 10^{-3}, 0.1, 0.5\}$ represented by violet, red, yellow, blue and green lines respectively. The black thick and dashed lines show the equilibrium distribution of WIMP and pFIMP respectively.

of DM yield as a function of x in Figures. 5 (a) and (b) for two different mass hierarchies. Red and violet dotted lines represent the pure FIMP scenario when $Y_2 = \{10^{-12}, 10^{-8}\}$ respectively. With larger Y_2 , conversion from WIMP to FIMP and consequently the FIMP yield increases. However, in this region, the FIMP still freezes-in. With Y_2 increasing further, the FIMP yield thermalises to equilibrium number density and enters into the pFIMP regime (yellow, blue and green dashed lines) to freeze-out subsequently. The pFIMP dynamics has been discussed in details in [51]. In Fig. 6(a), we show the allowed parameter space in $\delta m - Y_2$ plane, where the total relic adds to the observed one. The percentage contribution of the pFIMP (ϕ) is shown in the color axis. Note that, δm here is the mass difference between the two DM's. One can see, when $\delta m > 0$, i.e. the pFIMP is heavier than the WIMP, the decrease in δm increase the pFIMP-WIMP conversion significantly and therefore, the relative contribution of pFIMP to the total relic decreases. On the other hand, for the opposite hierarchy, i.e. $m_{\phi} < m_{\chi_1}$, increasing Y_2 will increase WIMP-pFIMP conversion thereby increasing pFIMP contribution to the total relic density.

In Fig. 6(b), we show the relic density allowed parameter space in $Y_2 - \Delta m$ plane. Here, Δm is the mass difference between the second lightest fermionic dark sector particle χ_2 and the WIMP DM χ_1 . We see that $\Delta m \lesssim 10$ GeV is required so that co-annihilation reduces χ_1 relic to the correct ballpark for pFIMP ϕ to saturate the rest of it. With larger Y_2 , the relative contribution of ϕ to the total relic density increases with more $\chi_1 \rightarrow \phi$ conversion.

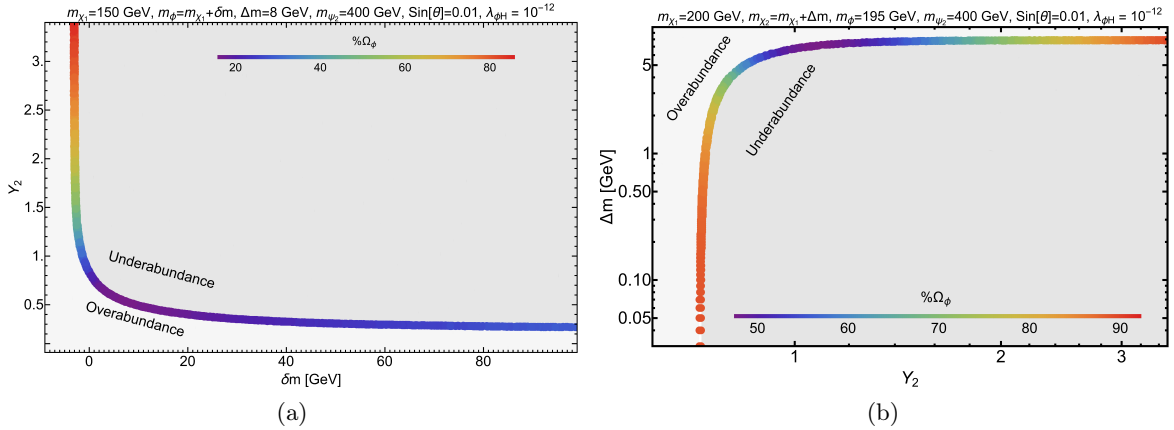


Figure 6: Parameter space allowed by the observed relic ($0.1188 \leq \Omega_{\text{DM}} h^2 \leq 0.1212$) in (a) $\delta m - Y_2$ plane (b) $Y_2 - \Delta m$ plane. In both the figures percentage contribution of pFIMP (Ω_ϕ) is shown in the color bar. Parameters kept fixed are mentioned in the figure heading.

4.2 Direct detection prospect

Now we delve into the direct search prospect of the two component DM's, which is our key focus in this study. First we will briefly discuss the direct detection of the WIMP and then explore the pFIMP case in detail.

4.2.1 Direct detection of WIMP

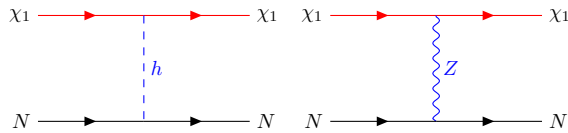


Figure 7: The Feynman diagrams for the direct detection of WIMP (χ_1).

In our model, the spin-independent direct detection cross section for WIMP χ_1 ($\sigma_{\chi_1 N}^{\text{SI}}$) gets major contribution from Z and Higgs-mediated t -channel diagrams (Fig. 7) and therefore the singlet-doublet mixing parameter $\sin \theta$ plays an important role, apart from the DM mass m_{χ_1} . The Z mediated contribution is required to be small to abide by the non-observation of a spin independent direct search of the DM. This is possible when the singlet doublet mixing ($\sin \theta$) is small, since the effective coupling involved in the Z mediated vertex is $\lambda_{Z\bar{\chi}_1\chi_1} = \frac{m_Z}{v} \sin^2 \theta$, whereas the effective Higgs coupling is $\lambda_{h\bar{\chi}_1\chi_1} = -\frac{Y_1}{\sqrt{2}} \sin 2\theta$.

In Fig. 8(a) and (b) we show the effective spin-independent direct detection cross-section ($\sigma_{\chi_1}^{\text{eff}}$) of the WIMP-like fermion DM χ_1 as a function of its mass (m_{χ_1}) for two different mass hierarchies. $\sigma_{\chi_1}^{\text{eff}}$ is defined [60] as follows,

$$\sigma_{\chi_1}^{\text{eff}} = \frac{\Omega_{\chi_1}}{\Omega_{\chi_1} + \Omega_\phi} \sigma_{\chi_1 N}^{\text{SI}}. \quad (4.9)$$

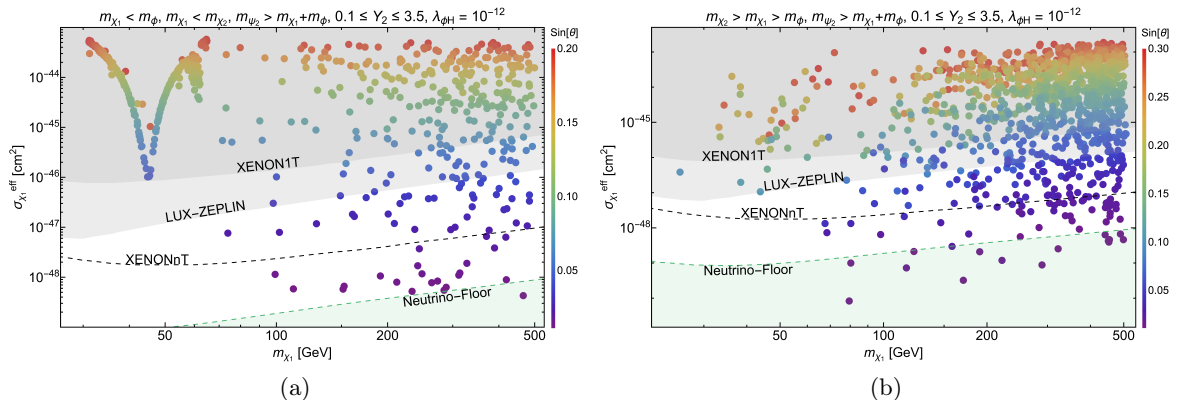


Figure 8: Effective spin-independent direct detection cross-section ($\sigma_{\chi_1}^{\text{eff}}$) for WIMP χ_1 for (a) $m_{\chi_1} < m_\phi$ and (b) $m_{\chi_1} > m_\phi$. All the points satisfy the present DM relic density bound $0.1188 \leq \Omega_{\chi_1} h^2 + \Omega_\phi h^2 \leq 0.1212$ via the combined contribution of both DM's. $\sin \theta$ is shown as color axis in both the figures. Other parameters kept fixed are shown in figure heading. The limits from XENON1T, LUX-ZEPLIN data and future sensitivities from XENONnT and Neutrino floor are shown.

In both figures 8 (a) and (b) $\sin \theta$ is shown as the color axis. It is clear that with increasing $\sin \theta$, with more doublet contribution, the direct detection cross-section for χ_1 increases. One finds in Fig. 8(a), when $m_{\chi_1} \lesssim 100$ GeV, only in the vicinity of Z -resonance, we get points allowed by relic density, but disfavoured from direct search data. But in the reverse hierarchy (Fig. 8(b)), the Z -resonance region is not particularly distinct. The reason behind this is the following. When $m_{\chi_1} > m_\phi$ the conversion channel from χ_1 to ϕ is open which helps χ_1 deplete considerably and become under-abundant, whereas when $m_{\chi_1} < m_\phi$, this conversion is kinematically disfavoured and therefore the under-abundance for χ_1 is achieved primarily near Z -resonance. Here too, small mass difference between χ_1 and χ_2 can facilitate co-annihilation and there is possibility of under-abundance with appropriate choice of Δm . The detailed calculation of direct detection cross-section of WIMP can be found in Appendix D. Broadly we see that WIMP mass is required to be larger than ~ 100 GeV with $\sin \theta \lesssim 0.1$.

4.2.2 Direct detection of pFIMP

The FIMP having negligible coupling with SM states is difficult to probe in direct search experiments. pFIMP on the other hand, despite having negligible couplings to SM, has a prospect of being detected at direct search experiments via substantial coupling to the WIMP. As discussed in Section 2.2, the pFIMP coupling to SM occurs via the WIMP-loop, which can have a non-negligible contribution to the elastic scattering between pFIMP and detector nucleon.

In Figure 9, we show the diagrams which contribute to the direct search cross-section of pFIMP (ϕ) in our model. The diagram (Figure 9 (left)) involving the Higgs portal coupling of pFIMP, contributes negligibly to the total amplitude. Figure 9 (middle) shows

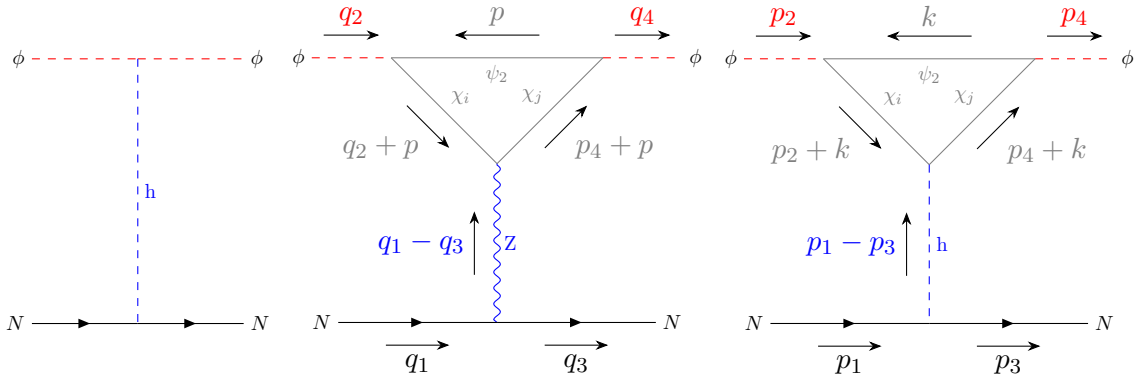


Figure 9: The (left) tree-level and (middle) and (right) one-loop Feynman diagram for the direct detection of pFIMP ϕ .

the WIMP-loop induced contribution with a t -channel Z mediator, whereas Figure 9 (right) shows the same with t -channel Higgs mediation.

The coupling that plays crucial role in determining the loop amplitude is the WIMP-pFIMP coupling (Yukawa coupling Y_2), which was also a key parameter in governing the pFIMP dynamics. On the other hand, one has to also remember that the loop contributions are also a direct consequence of the singlet-doublet mixing in our model. In the absence of mixing, the loop contribution to pFIMP-nucleon interaction vanishes. Therefore, not only the Yukawa coupling Y_2 , but also the Yukawa coupling Y_1 is crucial in this context. In addition, the mixing term is directly proportional to the mass difference between the WIMP and the second lightest dark sector particle ($m_{\chi_2} - m_{\chi_1}$), as we have seen in Equation (3.7). The smaller the mass difference, the weaker is the detectability of the pFIMP at direct detection experiments. Similar to the WIMP case, here too the Higgs mediated diagram contributes much more compared to the Z -mediated case, thanks to the small $\sin\theta$. For an order-of-magnitude estimate of the Higgs and Z mediated contributions, one can see Figure 16 and 18 in Appendix B. We would like to emphasize here that, we get an advantage by choosing a fermionic WIMP candidate over a scalar. It was shown in [47], that the pFIMP in a two-component scalar DM model, will have negligible contribution to the direct detection as the scalar loop-amplitude vanishes at the low transfer momentum limit (unless the WIMP is a warm DM in the keV mass-range). This is certainly not the case with fermion WIMP loop, which is our case. One can see the detailed calculation involving the fermion loop in Appendix B. Herein lies another very important motivation behind choosing our model. The detailed calculation of direct detection cross-section of pFIMP can be found in Appendix C, which we use for the parameter space scan discussed next.

In Fig. 10, we present the effective spin-independent direct detection cross-section (σ_ϕ^{eff}) of the pFIMP ϕ as a function of its mass (m_ϕ) for two different mass hierarchies. The definition of σ_ϕ^{eff} follows as before,

$$\sigma_\phi^{\text{eff}} = \frac{\Omega_\phi}{\Omega_{\chi_1} + \Omega_\phi} \sigma_{\phi N}^{\text{SI}}. \quad (4.10)$$

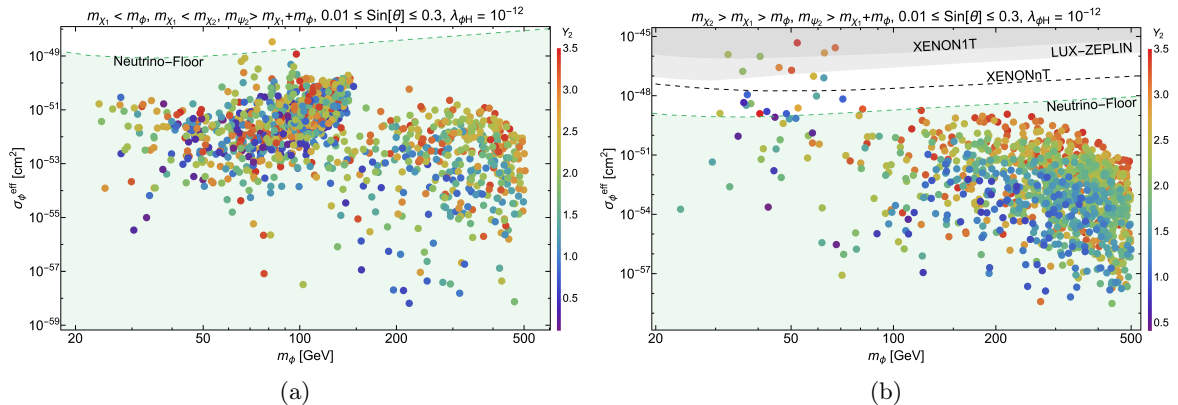


Figure 10: Effective spin-independent direct detection cross-section (σ_ϕ^{eff}) for pFIMP ϕ for (a) $m_{\chi_1} < m_\phi$ and (b) $m_{\chi_1} > m_\phi$. All the points satisfy the present DM relic density bound $0.1188 \leq \Omega_{\chi_1} h^2 + \Omega_\phi h^2 \leq 0.1212$ via the combined contribution of both DM's. Y_2 is shown as the color axis in both figures. Other parameters kept fixed are shown in figure heading. The limits from XENON1T, LUX-ZEPLIN data and future sensitivities from XENONnT and Neutrino floor are shown.

Since the tree-level coupling of ϕ with Higgs is extremely small $\lambda_{\phi H} \sim 10^{-12}$, the major contribution to σ_ϕ^{eff} comes from the fermion-loop induced diagrams (Fig. 9). Therefore, the parameters Δm , Y_2 and $\sin\theta$ play a crucial role. In order to achieve considerable direct detection cross-section a large Δm is desirable, as already pointed out. On the other hand, large Δm in turn means the absence of co-annihilation and therefore, over-abundance of χ_1 . This situation is evident in Figure 10(a), where the parameter space allowed by observed relic density immediately implies direct detection cross-section for the pFIMP below the neutrino floor. This tension is relaxed when $m_{\chi_1} > m_\phi$, since in this case the conversion channel from χ_1 to ϕ becomes kinematically favoured and under-abundance of χ_1 is possible even with large Δm . This in turn ensures moderate direct search cross-section ($10^{-49} - 10^{-47}$) for pFIMP ϕ with mass $\lesssim 100$ GeV for the next generation direct detection experiments like Xenon-nT (projected limit 10^{-49} cm²) to probe such cases, as shown in Figure 10(b). Hereby, we draw a crucial inference that $m_{\chi_1} > m_\phi$ is more favorable scenario for the detection of pFIMP, as compared to the inverse hierarchy.

Having discussed the individual aspects of WIMP and pFIMP direct detection, we would also like to make a connection between the two. In Figure 11, we have shown the allowed parameter space which respect the present relic density and direct detection (LUX-ZEPLIN) bound in $m_{\chi_1} - m_\phi$ plane. The color axis represents the effective spin-independent pFIMP-nucleon scattering cross-section, σ_ϕ^{eff} , in cm² in Log scale. It has been shown in [51], when $m_{\chi_1} > m_\phi$, WIMP-pFIMP conversion is significant via large Y_2 as well as via small mass difference between the WIMP and pFIMP. Furthermore, the contribution of ϕ to total relic in this case increases due to χ_1 to ϕ conversion, and therefore the effective direct detection too cross-section increases. In addition, if χ_1 is in the Z resonance, under-abundance of χ_1 becomes further enhanced and it becomes easier to achieve large Δm and consequently

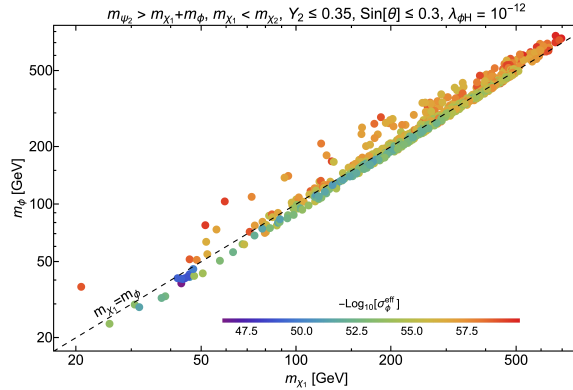


Figure 11: Allowed parameter space in $m_{\chi_1} - m_{\phi}$ plane, which respect the present observed relic density as well as have sensitivities for future direct detection experiments beyond LUX-ZEPLIN bound. The color axis represents the effective spin-independent pFIMP-nucleon scattering cross-section, $\sigma_{\phi}^{\text{eff}}$ in cm^2 in Log scale.

large direct detection cross-section for the pFIMP (blue points in the vicinity of Z resonance in Fig. 11). For the inverse hierarchy on the other hand, the under-abundance of WIMP is solely dependent on its co-annihilation and therefore, large Δm values are disfavoured, resulting in small direct detection cross-section for the pFIMP. We have checked that even with χ_1 in the vicinity Z resonance, the dependence on co-annihilation is not relaxed and therefore, direct detection cross-section for the pFIMP remains below the neutrino floor for almost the entire parameter space.

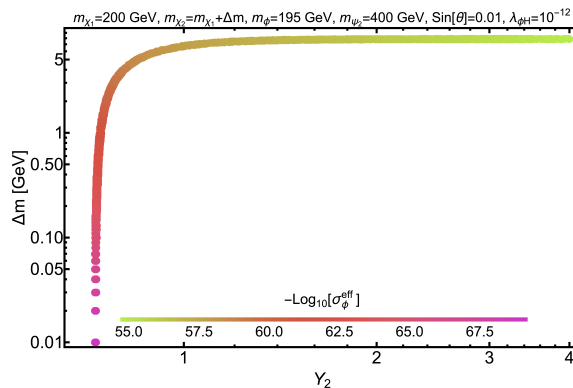


Figure 12: Parameter space allowed by observed relic and direct search in $Y_2 - \Delta m$ plane, where the spin-independent effective DM-nucleon elastic scattering cross-section of scalar DM ($\sigma_{\phi}^{\text{eff}}$ in cm^2) is shown as the color axis in Log scale.

In Fig. 12, we show the relic density and direct search allowed points in $Y_2 - \Delta m$ plane, with the color axis denoting the direct detection cross-section of the pFIMP ϕ . As discussed before large Δm will imply enhanced contribution from the fermion loop (see Figure 9). Therefore the spin-independent pFIMP-nucleon cross-section will increase with increasing Δm , which is evident from the transition in color in Figure 12. Needless to say, increasing

Y_2 is also crucial in obtaining enhanced contribution of ϕ to σ_ϕ^{eff} . Increasing Δm can also enhance the direct detection contribution of pFIMP. However, the requirement from observed relic forbids us to go beyond $\Delta m \sim 10$ GeV, a restriction which can be relaxed in the Z -resonance region, as pointed out earlier.

4.3 Indirect detection possibility

Similar to direct detection of pFIMP, one may also look for indirect signal evidence of pFIMP, analysing the photon flux [61] in the existing and future indirect detection experiments such as Fermi-LAT [62], SK [63], H.E.S.S [64], IceCube [65–67] etc. We have considered the recent data for DM annihilation channels to $b\bar{b}$, $\tau^+\tau^-$ and W^+W^- from various experiments and study their effect on our model parameter space. The strongest bounds come from the $b\bar{b}$ annihilation channel. The effective annihilation cross-section of a DM pair to $b\bar{b}$ final state is given as follows [68, 69],

$$\langle\sigma v\rangle_{\text{DM DM}\rightarrow b\bar{b}}^{\text{ID}} = \frac{\Omega_{\text{DM}}^2}{(\Omega_{\chi_1} + \Omega_\phi)^2} \langle\sigma v\rangle_{\text{DM DM}\rightarrow b\bar{b}}. \quad (4.11)$$

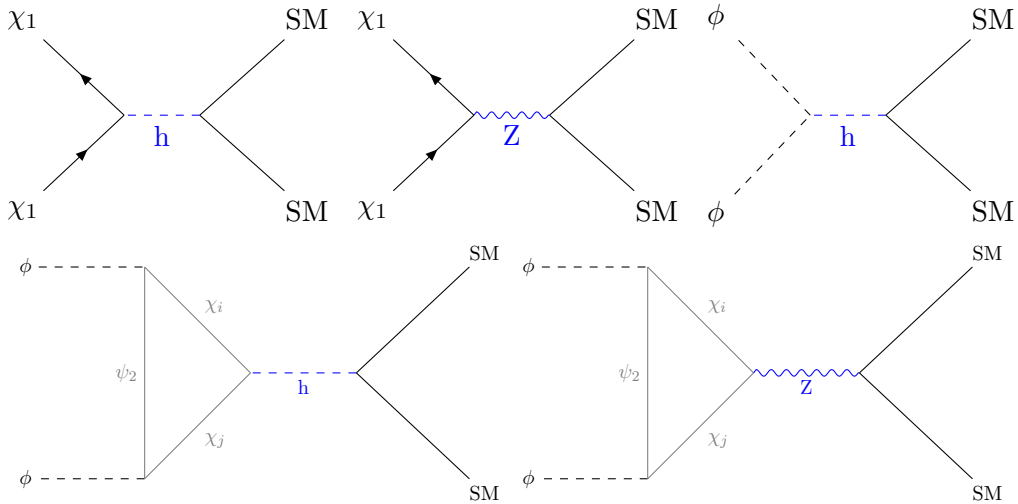


Figure 13: The Tree-level (left) and one-loop (right) Feynman diagrams for the Indirect detection of WIMP (χ_1) and pFIMP (ϕ).

In Figure 13, we show the processes that contribute to the aforementioned annihilation channels. We can see that the WIMP-loop induced diagrams take part in pFIMP annihilation, similar to the direct search case.

In Figure 14, we plot the quantity $\langle\sigma v\rangle_{\text{DM DM}\rightarrow b\bar{b}}^{\text{ID}}$ as a function of DM mass for WIMP (Figure 14(a)) and pFIMP (Figure 14(b)). The color axis denotes effective direct detection cross-section for pFIMP (σ_ϕ^{eff}). All the points in both the plots satisfy the observed relic and LUX-ZEPLIN bound. It is evident from the figures that the entire parameter space is allowed by indirect bound from Fermi-LAT (black dashed line) and can be probed at future experiments. Interestingly, the region that is most sensitive to the future indirect detection experiments are in the vicinity of Z -resonance. The same points produce maximum direct

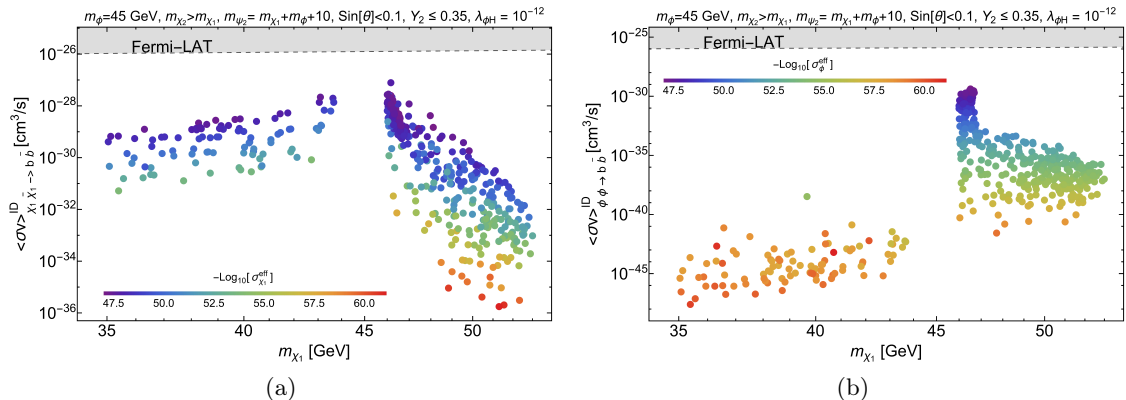


Figure 14: DM annihilation cross-section to $b\bar{b}$, $\langle\sigma v\rangle_{\chi_1\bar{\chi}_1\rightarrow b\bar{b}}^{\text{ID}}$ and $\langle\sigma v\rangle_{\phi\phi\rightarrow b\bar{b}}^{\text{ID}}$ as a function of DM mass. The color axis denotes effective direct detection cross-section for pFIMP ($\sigma_{\phi}^{\text{eff}}$). All points in $\sigma^{\text{ID}} - m_{\chi_1}$ plane satisfy observed relic and LUX-ZEPLIN bound for both WIMP and pFIMP. Grey shaded region is excluded by DM annihilation to $b\bar{b}$ search at Fermi-LAT [62, 70] and H.E.S.S [64] data.

search cross-section for the pFIMP (dark blue points in Figure 14(b)) and thereby yield best discovery potential.

5 Conclusion

Our focus is on a two-component DM scenario involving a thermal WIMP and a non-thermal FIMP having negligible interaction with SM. When the interaction between WIMP and FIMP becomes of weak interaction strength, the FIMP thermalises and freezes-out just like the WIMP. We categorized such DM candidates as pseudo-FIMP (pFIMP) and explored various aspects of this mechanism in our earlier work [51] in a model independent manner. In this work, we focus on a specific two component DM model to analyze the parameter space on the pFIMP region. The two different mass hierarchies present interesting dynamics as well as detection possibilities.

A crucial aspect of this work is to explore the possibility of detection of pFIMP in direct and indirect search experiments. It is well-known that a FIMP having tiny coupling to SM states, evades both present and future (projected) direct detection bounds. However, the pFIMP, aided by its significant interaction with the WIMP, can have considerable DM-nucleon cross-section at the direct search experiments. Although, the pFIMP has no direct connection to the SM, it can produce WIMP-loop induced amplitudes, which can bring the pFIMP under future experimental sensitivities. Having identified all such one-loop possibilities with scalar, fermion and vector boson particles as WIMP and pFIMP, we choose a specific model which is likely to provide a better pFIMP direct and indirect search sensitivity.

Our model consists of a fermion DM as WIMP which is an admixture of a singlet and a doublet. The pFIMP is a scalar singlet having negligible Higgs portal interaction

and a substantial WIMP-pFIMP conversion via Yukawa interaction. We have scanned the parameter space of our model and identified the region which is most sensitive to both direct and indirect search experiments. We found that, one of the mass hierarchies, where WIMP is heavier than pFIMP, is more favored in terms of its direct detection. On the other hand, in our model, a substantial mass difference between the WIMP and the second lightest dark sector particle, which is directly related to the singlet-doublet mixing, is required for a better detection prospect. Interestingly, the WIMP mass range in the Z -resonance region, turns out to be most sensitive in both direct and indirect searches. Importantly, the WIMP being a fermion in this model, also helps to generate a significant loop-induced amplitude. However, we do not claim that our model is the only scenario that is conducive for detecting a pFIMP. There is a plethora of possibilities, already outlined briefly in the beginning of this work, where similar analyses can be performed to study the rich phenomenology therein.

One of the crucial features of WIMP-pFIMP set up to address the correct relic density is to have the mass difference between the two around $\lesssim 10$ GeV. Therefore, we expect two DM signals in the same mass range. While this is very predictive in one hand, to disentangle them in such cases provide another important challenge ahead. The collider search prospect for pFIMP can similarly be studied involving a WIMP loop. This will be taken up in a future analysis.

Acknowledgments: SB and JL acknowledge the grant CRG/2019/004078 from SERB, Govt. of India.

Appendix

A BEQ with Coannihilation of dark matter in Wimp-Fimp framework

Let us consider, n_i dark sector particles have the same Z_2 symmetry, and their masses are m_i (m_1 being the mass of the stable DM), internal d.o.f g_i . The evolution of the number density n_i of particle i can be written as

$$\dot{n}_i + 3Hn_i = - \sum_j \langle \sigma v \rangle_{ij \rightarrow \text{SM}} \left(n_i n_j - n_i^{\text{eq}} n_j^{\text{eq}} \right) \quad (\text{A.1})$$

Since all these dark sector particles with $i > 1$, will eventually decay into the stable DM candidate after their respective freeze-out. Therefore the total DM density will be result of the combined yield of all the dark sector particles. Therefore, its final abundance(n) can be described by the sum of the density of all dark sector particle that transform under same Z_2 symmetry as the DM.

$$n = \sum_i n_i \quad (\text{A.2})$$

The corresponding evolution equation for n therefore can be written as follows [54, 59], without solving n_i BEQ simultaneously.

$$\dot{n} = -3Hn - \sum_{i,j} \langle \sigma v \rangle_{ij \rightarrow \text{SM}} \left(n_i n_j - n_i^{\text{eq}} n_j^{\text{eq}} \right) \quad (\text{A.3})$$

We have assumed that n_i dark sector particles are initially in thermal bath with SM via annihilation process. As the n_i remains in thermal equilibrium, and in particular their ratios follow their equilibrium value, we use the relation $\frac{n_i}{n} = \frac{n_i^{\text{eq}}}{n^{\text{eq}}}$ and the Eq. A.3 becomes,

$$\begin{aligned} \dot{n} &= -3Hn = - \sum_{ij} \langle \sigma v \rangle_{ij \rightarrow \text{SM}} \left(n_i^{\text{eq}} \frac{n}{n^{\text{eq}}} n_j^{\text{eq}} \frac{n}{n^{\text{eq}}} - n_i^{\text{eq}} n_j^{\text{eq}} \right) \\ &= - \sum_{ij} \langle \sigma v \rangle_{ij \rightarrow \text{SM}} \frac{n_i^{\text{eq}} n_j^{\text{eq}}}{n^{\text{eq}^2}} \left(n^2 - n^{\text{eq}^2} \right) \\ &= - \langle \sigma v \rangle_{\text{SM}}^{\text{eff}} \left(n^2 - n^{\text{eq}^2} \right) \end{aligned} \quad (\text{A.4})$$

where,

$$\langle \sigma v \rangle^{\text{eff}} = \sum_{i,j} \langle \sigma v \rangle_{ij} \frac{n_i^{\text{eq}} n_j^{\text{eq}}}{n^{\text{eq}^2}} \quad \text{and} \quad n^{\text{eq}} = \sum_i n_i^{\text{eq}} \quad (\text{A.5})$$

Following Eq. A.5, it is straightforward to calculate the $\langle \sigma v \rangle^{\text{eff}}$ for all possible channels in Eqs. 4.1 and 4.2.

$$\langle \Gamma \rangle_{\psi_2 \rightarrow \chi_1 \phi}^{\text{eff}} = \sum_i \langle \Gamma \rangle_{\psi_2 \rightarrow i \phi} \quad (\text{A.6})$$

$$\langle \sigma v \rangle_{\chi_1 \bar{\psi}_2 \rightarrow h \phi}^{\text{eff}} = \left[\sum_i g_i m_i^2 K_2 \left(\frac{m_i}{T} \right) \right]^{-1} \sum_i 2 \langle \sigma v \rangle_{i \bar{\psi}_2 \rightarrow h \phi} g_i m_i^2 K_2 \left(\frac{m_i}{T} \right) \quad (\text{A.7})$$

$$\langle \sigma v \rangle_{\phi}^{\text{eff}} = \left[\sum_i g_i m_i^2 K_2 \left(\frac{m_i}{T} \right) \right]^{-2} \sum_{i,j} 2 \langle \sigma v \rangle_{ij \rightarrow \phi \phi} g_i g_j m_i^2 m_j^2 K_2 \left(\frac{m_i}{T} \right) K_2 \left(\frac{m_j}{T} \right) \quad (\text{A.8})$$

$$\langle \sigma v \rangle_{\psi_2}^{\text{eff}} = \left[\sum_i g_i m_i^2 K_2 \left(\frac{m_i}{T} \right) \right]^{-2} \sum_{i,j} 2 \langle \sigma v \rangle_{ij \rightarrow \psi_2 \bar{\psi}_2} g_i g_j m_i^2 m_j^2 K_2 \left(\frac{m_i}{T} \right) K_2 \left(\frac{m_j}{T} \right) \quad (\text{A.9})$$

$$\langle \sigma v \rangle_{\text{SM}}^{\text{eff}} = \left[\sum_i g_i m_i^2 K_2 \left(\frac{m_i}{T} \right) \right]^{-2} \sum_{i,j} 2 \langle \sigma v \rangle_{ij \rightarrow \text{SM SM}} g_i g_j m_i^2 m_j^2 K_2 \left(\frac{m_i}{T} \right) K_2 \left(\frac{m_j}{T} \right) \quad (\text{A.10})$$

B Relevant Fermion Loop Calculations for direct search

We consider first the three-point vertex and its one loop contribution, for the $\phi\phi h$ interaction, which plays crucial role in the direct detection of the pFIMP. The 1-loop amplitude part can be written as,

$$\mathbb{L}_h = -i\lambda_{h\phi\phi} + \sum_{i,j=1,2} \Gamma_{ij}^{1\text{-loop}} + \delta_{ij}^\lambda \quad (\text{B.1})$$

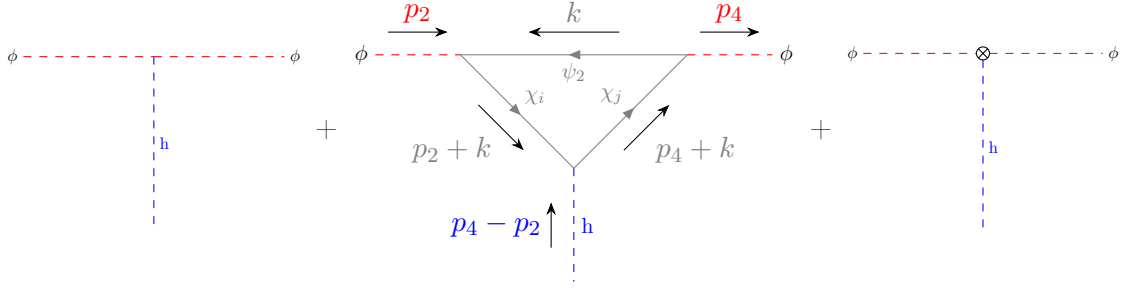


Figure 15: Tree-level, one-loop and counter-term interaction vertex for the interaction term $h\phi\phi$ where $\{i, j = 1, 2\}$ [71, 72].

We have assumed that at tree level $\lambda_{\phi H}$ is very small w.r.t other couplings. The one-loop diagram contributes to the $h\phi\phi$ vertex is given in the middle of Fig. 15 and the amplitude is given by,

$$\begin{aligned}
\Gamma_{ij}^{1-\text{loop}} &= \int \frac{d^4 k}{(2\pi)^4} (-1) \text{Tr} \left[\frac{(-i\lambda_{\phi\psi_2\chi_j})i(\not{k} + m_{\psi_2})}{[k^2 - m_{\psi_2}^2 + i\epsilon]} \frac{(-i\lambda_{\phi\psi_2\chi_i})i(\not{p}_2 + \not{k} + m_{\chi_i})}{[(p_2 + k)^2 - m_{\chi_i}^2 + i\epsilon]} \frac{(-i\lambda_{h\chi_i\chi_j})i(\not{p}_4 + \not{k} + m_{\chi_j})}{[(p_4 + k)^2 - m_{\chi_j}^2 + i\epsilon]} \right] \\
&= -\lambda_{h\chi_i\chi_j} \lambda_{\phi\psi_2\chi_j} \lambda_{\phi\psi_2\chi_i} \int \frac{d^4 k}{(2\pi)^4} \frac{\text{Tr} \left[(\not{k} + m_{\psi_2})(\not{p}_2 + \not{k} + m_{\chi_i})(\not{p}_4 + \not{k} + m_{\chi_j}) \right]}{[k^2 - m_{\psi_2}^2 + i\epsilon] [(p_2 + k)^2 - m_{\chi_i}^2 + i\epsilon] [(p_4 + k)^2 - m_{\chi_j}^2 + i\epsilon]} \\
&= -4 \int \frac{d^4 k}{(2\pi)^4} \frac{m_{\psi_2}(p_2 \cdot p_4 + k \cdot p_4 + k \cdot p_2 + k^2) + m_{\chi_i}(k \cdot p_4 + k^2) + m_{\chi_j}(k \cdot p_2 + k^2) + m_{\chi_i} m_{\chi_j} m_{\psi_2}}{[k^2 - m_{\psi_2}^2 + i\epsilon] [(k + p_2)^2 - m_{\chi_i}^2 + i\epsilon] [(k + p_4)^2 - m_{\chi_j}^2 + i\epsilon]} \quad (\text{B.2}) \\
&\quad \times \lambda_{h\chi_i\chi_j} \lambda_{\phi\psi_2\chi_j} \lambda_{\phi\psi_2\chi_i} \\
&= -4 \int \frac{d^4 k}{(2\pi)^4} \frac{m_{\chi_i} m_{\chi_j} m_{\psi_2} + m_{\psi_2}(m_\phi^2 - \frac{t}{2}) + (m_{\chi_i} + m_{\chi_j} + m_{\psi_2})k^2 + (m_{\psi_2} + m_{\chi_j})k \cdot p_2 + (m_{\psi_2} + m_{\chi_i})k \cdot p_4}{[k^2 - m_{\psi_2}^2 + i\epsilon] [(k + p_2)^2 - m_{\chi_i}^2 + i\epsilon] [(k + p_4)^2 - m_{\chi_j}^2 + i\epsilon]} \\
&\quad \times \lambda_{h\chi_i\chi_j} \lambda_{\phi\psi_2\chi_j} \lambda_{\phi\psi_2\chi_i}
\end{aligned}$$

$$\begin{aligned}
&\left[\text{Where, } l = k + yp_2 + zp_4, \Delta_{ij} = (y+z)(y+z-1)m_\phi^2 - tyz + xm_{\psi_2}^2 + ym_{\chi_i}^2 + zm_{\chi_j}^2, \right. \\
&\delta m_{ij} = m_{\psi_2} \left(m_{\chi_i} m_{\chi_j} + m_\phi^2(1-y-z)^2 - \frac{t}{2}(1-y-z+2yz) \right) + m_\phi^2(m_{\chi_i} + m_{\chi_j})(y+z)(y+z-1) + \\
&\left. \frac{t}{2}m_{\chi_i}y(1-2z) + \frac{t}{2}m_{\chi_j}z(1-2y), c_{ij} = m_{\psi_2} + m_{\chi_i} + m_{\chi_j} \right].
\end{aligned}$$

As $l \cdot p_{2,4}$ are odd under $l \rightarrow -l$ while the rest of the integrand, is even.

$$\begin{aligned}
\Gamma_{ij}^{1\text{-loop}} &= -8\lambda_{h\chi_i\chi_j}\lambda_{\phi\psi_2\chi_j}\lambda_{\phi\psi_2\chi_i}\int\frac{d^4l}{(2\pi)^4}\int_0^1dx\,dy\,dz\frac{\delta m_{ij}+c_{ij}l^2}{(l^2-\Delta_{ij}+i\epsilon)^3}\delta(x+y+z-1) \\
&= -8\lambda_{h\chi_i\chi_j}\lambda_{\phi\psi_2\chi_j}\lambda_{\phi\psi_2\chi_i}\mu^{4-d}\int\frac{d^d l}{(2\pi)^d}\int_0^1dx\,dy\,dz\frac{\delta m_{ij}+c_{ij}l^2}{(l^2-\Delta_{ij}+i\epsilon)^3}\delta(x+y+z-1) \\
\text{Where } \mu &\text{ is dimension regularization parameter (basically a mass scale) introduced to keep } \lambda \\
&\text{ dimensionless and } d=4-2\epsilon \text{ in the limit, } \epsilon\rightarrow 0_+. \\
&= -8\lambda_{h\chi_i\chi_j}\lambda_{\phi\psi_2\chi_j}\lambda_{\phi\psi_2\chi_i}\mu^{4-d}\int_0^1dx\,dy\,dz\left[\delta m_{ij}\frac{(-1)^3i}{(4\pi)^{d/2}}\frac{\Gamma(3-d/2)}{\Gamma(3)}\left(\frac{1}{\Delta_{ij}}\right)^{3-d/2}+\right. \\
&\quad \left. c_{ij}\frac{(-1)^{3-1}i}{(4\pi)^{d/2}}\frac{d}{2}\frac{\Gamma(3-d/2-1)}{\Gamma(3)}\left(\frac{1}{\Delta_{ij}}\right)^{3-d/2-1}\right]\delta(x+y+z-1) \\
&= 8i\lambda_{h\chi_i\chi_j}\lambda_{\phi\psi_2\chi_j}\lambda_{\phi\psi_2\chi_i}\int_0^1dx\,dy\,dz\left[\frac{\delta m_{ij}}{32\pi^2}\frac{\Gamma(1+\epsilon)}{\Delta_{ij}^{1+\epsilon}}(4\pi\mu^2)^\epsilon-\frac{c_{ij}}{32\pi^2}(2-\epsilon)\frac{\Gamma(\epsilon)}{\Delta_{ij}^\epsilon}(4\pi\mu^2)^\epsilon\right]\delta(x+y+z-1).
\end{aligned} \tag{B.3}$$

Around $\epsilon\rightarrow 0_+$ limit we have the expansions,

$$\begin{aligned}
\Gamma(\epsilon) &\simeq \frac{1}{\epsilon}-\gamma_E+\mathcal{O}(\epsilon), \\
\frac{1}{\Delta^\epsilon} &\simeq 1-\frac{\epsilon}{2}\ln\Delta^2+\mathcal{O}(\epsilon), \\
\mu^\epsilon &\simeq 1+\frac{\epsilon}{2}\ln\mu^2+\mathcal{O}(\epsilon).
\end{aligned} \tag{B.4}$$

where $\gamma_E\approx 0.5772156649$ is the Euler-Mascheroni constant. Then,

$$\Gamma_{ij}^{1\text{-loop}} = \frac{i}{4\pi^2}\lambda_{h\chi_i\chi_j}\lambda_{\phi\psi_2\chi_j}\lambda_{\phi\psi_2\chi_i}\int_0^1dx\,dy\,dz\left[\frac{\delta m_{ij}}{\Delta_{ij}}-2c_{ij}\underbrace{\left(\frac{1}{\epsilon}-\gamma_E+\ln[4\pi]-\frac{1}{2}+\ln\frac{\mu^2}{\Delta_{ij}}\right)}_{\text{counter term}}\right]+\mathcal{O}(\epsilon) \times\delta(x+y+z-1). \tag{B.5}$$

Clearly, in the $\overline{\text{MS}}$ renormalization scheme the counter term δ_{ij}^λ has to be fixed at the following value to cancel the pole in the Eq. B.5,

$$\delta_{ij}^\lambda = i\lambda_{h\chi_i\chi_j}\lambda_{\phi\psi_2\chi_j}\lambda_{\phi\psi_2\chi_i}\frac{c_{ij}}{2\pi^2}\left(\frac{1}{\epsilon}-\gamma_E+\ln 4\pi\right). \tag{B.6}$$

and the total amplitude at $\epsilon\rightarrow 0$ becomes,

$$\mathbb{L}_h = -i\lambda_{h\phi\phi}+\frac{i}{4\pi^2}\sum_{i,j=1,2}\lambda_{h\chi_i\chi_j}\lambda_{\phi\psi_2\chi_j}\lambda_{\phi\psi_2\chi_i}\int_0^1dx\,dy\,dz\left[\frac{\delta m_{ij}}{\Delta_{ij}}+c_{ij}\left(1-2\ln\frac{\mu^2}{\Delta_{ij}}\right)\right]\delta(x+y+z-1). \tag{B.7}$$

with,

$$\begin{aligned}
\lambda_{\phi\psi_2\bar{\chi}_1} &= \lambda_{\phi\bar{\psi}_2\chi_1} = -Y_2\cos\theta, \\
\lambda_{\phi\psi_2\bar{\chi}_2} &= \lambda_{\phi\bar{\psi}_2\chi_2} = Y_2\sin\theta, \\
\lambda_{h\bar{\chi}_1\chi_1} &= -\frac{Y_1}{\sqrt{2}}\sin 2\theta, \\
\lambda_{h\bar{\chi}_2\chi_2} &= \frac{Y_1}{\sqrt{2}}\sin 2\theta, \\
\lambda_{h\bar{\chi}_1\chi_2} &= \lambda_{h\bar{\chi}_2\chi_1} = -\frac{Y_1}{\sqrt{2}}\cos 2\theta.
\end{aligned} \tag{B.8}$$

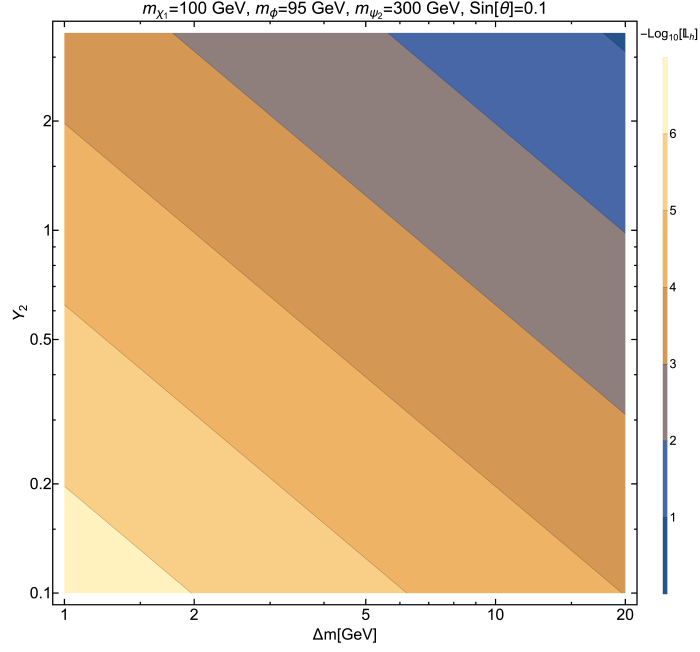


Figure 16: One-loop amplitude for the Higgs-mediated process.

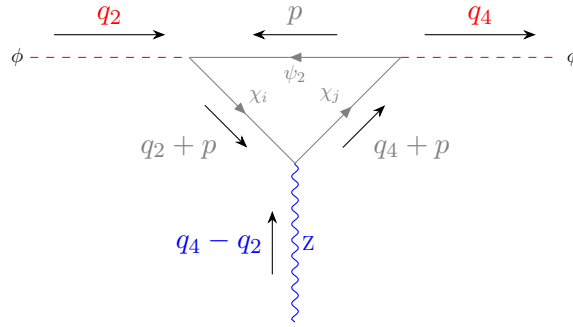


Figure 17: One-loop Feynman diagram for the interaction term $Z\phi\phi$ where $\{i, j = 1, 2\}$.

We present next the 1-loop contribution of the Z -mediated diagram to the pFIMP-nucleon cross-section.

$$\begin{aligned}
\mathbb{L}_\mu^{ij} &= (-1) \int \frac{d^4 p}{(2\pi)^4} \text{Tr} \left[\frac{(-i\lambda_{\phi\psi_2\chi_j})i(\not{p} + m_{\psi_2})}{[p^2 - m_{\psi_2}^2 + i\epsilon]} \frac{(-i\lambda_{\phi\psi_2\chi_i})i(\not{q}_2 + \not{p} + m_{\chi_i})}{[(q_2 + p)^2 - m_{\chi_i}^2 + i\epsilon]} \frac{(-i\gamma_\mu \lambda_{Z\chi_i\chi_j})i(\not{q}_4 + \not{p} + m_{\chi_j})}{[(q_4 + p)^2 - m_{\chi_j}^2 + i\epsilon]} \right] \\
&= -4\lambda_{\phi\psi_2\chi_j} \lambda_{\phi\psi_2\chi_i} \lambda_{Z\chi_i\chi_j} \int \frac{d^4 p}{(2\pi)^4} \left[\frac{(m_{\psi_2} m_{\chi_j} + p \cdot p + p \cdot q_4) q_{2\mu} + (m_{\psi_2} m_{\chi_i} + p \cdot p + p \cdot q_2) q_{4\mu}}{[p^2 - m_{\psi_2}^2 + i\epsilon] [(q_2 + p)^2 - m_{\chi_i}^2 + i\epsilon] [(q_4 + p)^2 - m_{\chi_j}^2 + i\epsilon]} \right. \\
&\quad \left. + \frac{(m_{\chi_i} m_{\chi_j} + m_{\psi_2} m_{\chi_i} + m_{\psi_2} m_{\chi_j} + p \cdot p - q_2 \cdot q_4) p_\mu}{[p^2 - m_{\psi_2}^2 + i\epsilon] [(q_2 + p)^2 - m_{\chi_i}^2 + i\epsilon] [(q_4 + p)^2 - m_{\chi_j}^2 + i\epsilon]} \right] \\
&\quad \left[\text{Using Feynman parametrization } l = p + yq_2 + zq_4, \text{ we define,} \right. \\
\Delta^{ij} &= (y+z)(y+z-1)m_\phi^2 - tyz + xm_{\psi_2}^2 + ym_{\chi_i}^2 + zm_{\chi_j}^2, \\
\delta m_\mu^{ij} &= [m_{\psi_2} m_{\chi_j} - (m_{\psi_2} m_{\chi_j} + m_{\psi_2} m_{\chi_i} + m_{\chi_i} m_{\chi_j})y + tyz(y-1) - m_\phi^2(z + (y-1)(y+z)^2)] q_{2\mu} + \\
&\quad [m_{\psi_2} m_{\chi_i} - (m_{\psi_2} m_{\chi_i} + m_{\psi_2} m_{\chi_j} + m_{\chi_i} m_{\chi_j})z + tyz(z-1) - m_\phi^2(y + (z-1)(y+z)^2)] q_{4\mu}, \\
c_\mu &= (1-y)q_{2\mu} + (1-z)q_{4\mu} \Big]. \\
&= -8\lambda_{\phi\psi_2\chi_j} \lambda_{\phi\psi_2\chi_i} \lambda_{Z\chi_i\chi_j} \int_0^1 dx dy dz \int \frac{d^4 l}{(2\pi)^4} \frac{\delta m_\mu^{ij} + c_\mu l^2 - 2yq_2^\alpha l_\alpha l_\mu - 2zq_4^\beta l_\beta l_\mu}{[l^2 - \Delta^{ij} + i\epsilon]^3} \delta(x+y+z-1) \tag{B.9}
\end{aligned}$$

using dimensional regularisation method we may write,

$$\begin{aligned}
&\equiv -8\lambda_{\phi\psi_2\chi_j} \lambda_{\phi\psi_2\chi_i} \lambda_{Z\chi_i\chi_j} \mu^{4-d} \int_0^1 dx dy dz \int \frac{d^d l}{(2\pi)^d} \frac{\delta m_\mu^{ij} + c_\mu l^2 - \frac{2}{d} yq_2^\alpha l^\alpha l_\mu - \frac{2}{d} zq_4^\beta l^\beta l_\mu}{[l^2 - \Delta^{ij} + i\epsilon]^3} \\
&\quad \times \delta(x+y+z-1) \\
&= 8i\lambda_{\phi\psi_2\chi_j} \lambda_{\phi\psi_2\chi_i} \lambda_{Z\chi_i\chi_j} \int_0^1 dx dy dz \left[\frac{\delta m_\mu^{ij} \Gamma(1+\epsilon)}{32\pi^2 \Delta^{ij^{1+\epsilon}}} (4\pi\mu^2)^\epsilon \right. \\
&\quad \left. - (2-\epsilon) \frac{(4\pi\mu^2)^\epsilon \Gamma(\epsilon)}{32\pi^2 \Delta^{ij^\epsilon}} c_\mu + \frac{(4\pi\mu^2)^\epsilon \Gamma(\epsilon)}{32\pi^2 \Delta^{ij^\epsilon}} (yq_{2\mu} + zq_{4\mu}) \right] \delta(x+y+z-1) \\
&= \frac{i}{4\pi^2} \lambda_{\phi\psi_2\chi_j} \lambda_{\phi\psi_2\chi_i} \lambda_{Z\chi_i\chi_j} \int_0^1 dx dy dz \left[\delta m_\mu^{ij} \frac{\Gamma(1+\epsilon)}{\Delta^{ij^{1+\epsilon}}} (4\pi\mu^2)^\epsilon \right. \\
&\quad \left. - (2c_\mu - yq_{2\mu} - zq_{4\mu}) \frac{\Gamma(\epsilon)}{\Delta^{ij^\epsilon}} (4\pi\mu^2)^\epsilon + c_\mu \epsilon \frac{\Gamma(\epsilon)}{\Delta^{ij^\epsilon}} (4\pi\mu^2)^\epsilon \right] \delta(x+y+z-1) \\
&= \frac{i}{4\pi^2} \lambda_{\phi\psi_2\chi_j} \lambda_{\phi\psi_2\chi_i} \lambda_{Z\chi_i\chi_j} \int_0^1 dx dy dz \left[\frac{\delta m_\mu^{ij}}{\Delta^{ij}} - (2c_\mu - yq_{2\mu} - zq_{4\mu}) \left(\frac{1}{\epsilon} - \gamma_E + \ln[4\pi\mu^2] - \ln \Delta^{ij} \right) \right. \\
&\quad \left. + c_\mu + \mathcal{O}(\epsilon) \right] \delta(x+y+z-1).
\end{aligned}$$

Where,

$$\begin{aligned}
\lambda_{\phi\psi_2\bar{\chi}_1} &= \lambda_{\phi\psi_2\chi_1} = -Y_2 \cos \theta, \\
\lambda_{\phi\psi_2\bar{\chi}_2} &= \lambda_{\phi\psi_2\chi_2} = Y_2 \sin \theta, \\
\lambda_{Z\bar{\chi}_1\chi_1} &= \frac{g}{2 \cos \theta_w} \sin^2 \theta = \frac{m_Z}{v} \sin^2 \theta, \\
\lambda_{Z\bar{\chi}_2\chi_2} &= \frac{g}{2 \cos \theta_w} \cos^2 \theta = \frac{m_Z}{v} \cos^2 \theta, \\
\lambda_{Z\bar{\chi}_1\chi_2} &= \lambda_{Z\bar{\chi}_2\chi_1} = \frac{g}{2 \cos \theta_w} \sin \theta \cos \theta = \frac{m_Z}{v} \sin \theta \cos \theta.
\end{aligned} \tag{B.10}$$

and the total loop amplitude becomes,

$$\begin{aligned}
\mathbb{L}_\mu^Z &= \sum_{i,j=1,2} \mathbb{L}_\mu^{ij} \\
&= \frac{i}{4\pi^2} \sum_{i,j=1,2} \lambda_{\phi\psi_2\chi_j} \lambda_{\phi\psi_2\chi_i} \lambda_{Z\chi_i\chi_j} \int_0^1 dx dy dz \left[\frac{\delta m_\mu^{ij}}{\Delta^{ij}} \right. \\
&\quad \left. - (2c_\mu - yq_{2\mu} - zq_{4\mu}) \left(\frac{1}{\epsilon} - \gamma_E + \ln[4\pi\mu^2] - \ln \Delta^{ij} \right) + c_\mu + \mathcal{O}(\epsilon) \right] \delta(x+y+z-1) \\
&\stackrel{\epsilon \rightarrow 0}{=} \frac{i}{4\pi^2} \sum_{i,j=1,2} \lambda_{\phi\psi_2\chi_j} \lambda_{\phi\psi_2\chi_i} \lambda_{Z\chi_i\chi_j} \int_0^1 dx dy dz \left[\frac{\delta m_\mu^{ij}}{\Delta^{ij}} + (2c_\mu - yq_{2\mu} - zq_{4\mu}) \ln \Delta^{ij} \right] \delta(x+y+z-1) \\
&\xrightarrow{m_{\chi_1}=m_{\chi_2}} 0 \\
&\xrightarrow{m_{\chi_1} \neq m_{\chi_2}} \mathbb{L}_Z(q_{2\mu} + q_{4\mu})
\end{aligned}$$

We have cross-checked our analytical solution with Package-X [73] and FeynCalc [74].

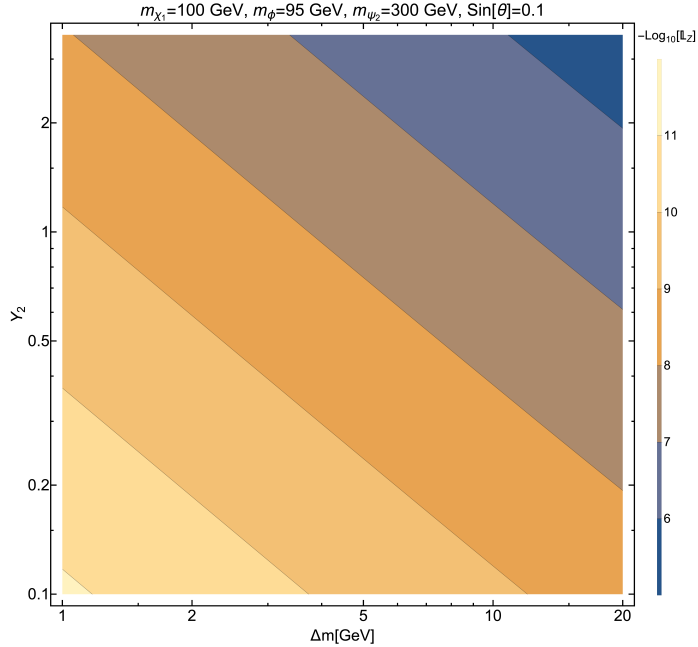


Figure 18: One-loop amplitude for the Z -mediated process.

C Calculation of direct detection cross-section of pFIMP

The Feynman diagrams for DM ϕ scattering off a nucleon at tree-level and one-loop level are shown in Fig. 9.

Higgs Mediated pFIMP-Nucleon Scattering:

For higgs mediator, the tree-level contribution will be negligible because of tiny $h\phi\phi$ coupling that we have assumed, justifiably, in the pFIMP scenario. The dominant Higgs-mediated contribution therefore comes from 1-loop diagram. The two interaction vertices involved in the loop-induced

Higgs-mediated process, are $\mathbb{L}_h h \phi \phi$ and $\frac{m_q}{v} h q \bar{q}$, the Effective Lagrangian at the parton level can be written as,

$$\mathcal{L}_{eff}^h = \mathbb{L}_h \frac{m_q}{v} \frac{1}{m_h^2} q \bar{q} \phi \phi = f_q^h q \bar{q} \phi \phi. \quad (\text{C.1})$$

The matrix element for a scattering $N \phi \rightarrow N \phi$ via Higgs-mediation, where N stands for nucleon, is the following:

$$i\mathcal{M}_{N\phi}^h = \alpha_N^h \left[\overline{u_N}(q_3) u_N(q_1) \right] 1 \quad (\text{C.2})$$

where α_N^h is the effective DM-nucleon coupling and the relation with quark level coupling is,

$$\frac{\alpha_N^h}{m_N} = \sum_{q=u,d,s} f_{T_q}^N \frac{f_q^h}{m_q} + \frac{2}{27} \left(1 - \sum_{q=u,d,s} f_{T_q}^N \right) \sum_{q=c,b,t} \frac{f_q^h}{m_q}. \quad (\text{C.3})$$

Where the nuclear form-factors are defined by [75, 76]

$$\langle N | m_q \bar{q} q | N \rangle \equiv m_N f_{T_q}^N \langle N | N \rangle \quad (q = u, d, s) \quad (\text{C.4})$$

Nucleon	$f_{T_u}^N$	$f_{T_d}^N$	$f_{T_s}^N$	$f_{T_G}^N$	$f_{T_c}^N$	$f_{T_b}^N$	$f_{T_t}^N$
Proton	0.018(5)	0.027(7)	0.037(17)	0.917(19)	0.078(2)	0.072(2)	0.069(1)
Neutron	0.013(3)	0.040(10)	0.037(17)	0.910(20)	0.078(2)	0.071(2)	0.068(2)

Table 3: Values of the $f_{T_{q,G}}^N$.

$$\begin{aligned} |\overline{\mathcal{M}_{N\phi}^h}|^2 &= \frac{1}{2} \sum_{\text{all spin}} |\mathcal{M}_{N\phi}^h|^2 \\ &= 4m_N^2 |\alpha_N^h|^2 \end{aligned} \quad (\text{C.5})$$

Z Mediated pFIMP-Nucleon Scattering:

The Effective Lagrangian for Z mediator direct search process can be written as,

$$\begin{aligned} \mathcal{L}_{eff}^Z &= \bar{q} \left[\frac{g}{\cos \theta_W} \gamma^\mu \frac{1}{2} (c_V^q - c_A^q \gamma^5) \right] q \frac{\mathbb{L}_Z}{m_Z} \phi(q_{2_\mu} + q_{4_\nu}) \phi && \text{SI + SD} \\ &\rightarrow \frac{m_Z}{v} c_V^q \frac{\mathbb{L}_Z}{m_Z} \bar{q} \gamma^\mu q \phi(q_{2_\mu} + q_{4_\mu}) \phi && \text{SI} \\ &= \frac{c_V^q}{v} \frac{\mathbb{L}_Z}{m_Z} \bar{q} \gamma^\mu q \phi(q_{2_\mu} + q_{4_\mu}) \phi \\ &= \frac{c_V^q}{v} \frac{\mathbb{L}_Z}{m_Z} \bar{q} \gamma^\mu q \phi(q_{2_\mu} + q_{4_\mu}) \phi \\ &= b_q^Z \bar{q} \gamma^\mu q \phi(q_{2_\mu} + q_{4_\mu}) \phi \end{aligned} \quad (\text{C.6})$$

The matrix element for DM nucleon scattering $N \phi \rightarrow N \phi$, is the following by assuming Let, $\mathbb{L}_\mu^Z = \mathbb{L}_Z(q_{2_\mu} + q_{4_\mu})$:

$$i\mathcal{M}_{N\phi}^Z = b_N^Z \left[\overline{u_N}(q_3) \gamma^\mu u_N(q_1) \right] (q_{2_\mu} + q_{4_\mu}) \quad (\text{C.7})$$

where b_N^Z is the DM-nucleon effective coupling. As the sea-quarks and the gluons do not contribute to the vector current. Only valence quark contributions all add up due to the conservation of the vector current which gives us, $b_p = 2b_u + b_d$ and $b_n = b_u + 2b_d$. So the relation effective DM-nucleon couplings with quark level coupling are [77],

$$\begin{aligned} b_p^Z &= 2b_u^Z + b_d^Z \\ b_n^Z &= b_u^Z + 2b_d^Z \end{aligned} \quad (\text{C.8})$$

with $b_q^Z = \frac{c_V^q}{v} \frac{\mathbb{L}_Z}{m_Z}$.

$$\overline{|\mathcal{M}_{N\phi}^Z|^2} = \frac{|b_N^Z|^2}{2} \text{Tr} \left[(\not{q}_3 + m_N) \gamma^\mu (\not{q}_1 + m_N) \gamma^\nu \right] (q_{2\mu} + q_{4\mu})(q_{2\nu} + q_{4\nu}) \quad (\text{C.9})$$

$$\begin{aligned} &= \frac{|b_N^Z|^2}{2} 4(q_1^\mu q_3^\nu + q_3^\mu q_1^\nu)(q_{2\mu} + q_{4\mu})(q_{2\nu} + q_{4\nu}) \\ &= 4|b_N^Z|^2 (q_1 \cdot q_2 + q_1 \cdot q_4) (q_3 \cdot q_2 + q_3 \cdot q_4) \\ &= 4|b_N^Z|^2 4m_\phi^2 m_N^2 \quad \text{as initially the nucleus is in rest, } q_1 \sim \{m_N, \vec{0}\} \end{aligned} \quad (\text{C.10})$$

The interference:

Let us now calculate the cross-term,

$$\begin{aligned} \overline{|\mathcal{M}_{N\phi}^Z|^\dagger |\mathcal{M}_{N\phi}^h|} &= \frac{1}{2} \sum_{\text{all spin}} [b_N^Z (\bar{u}_N(q_3) \gamma^\mu u_N(q_1)) (q_{2\mu} + q_{4\mu})]^\dagger [\alpha_N^h (\bar{u}_N(q_3) u_N(q_1)) 1] \\ &= \frac{b_N^Z \alpha_N^h}{2} \text{Tr} \left[\gamma^\mu (\not{q}_3 + m_N) (\not{q}_1 + m_N) \right] (q_{2\mu} + q_{4\mu}) \\ &= 2m_N b_N^Z \alpha_N^h (q_1 \cdot q_2 + q_1 \cdot q_4 + q_2 \cdot q_3 + q_3 \cdot q_4) \\ &= 2m_N b_N^Z \alpha_N^h 4m_\phi m_N \quad \text{as initially the nucleus is in rest, } q_1 \sim \{m_N, \vec{0}\} \\ &= 8m_N^2 m_\phi b_N^Z \alpha_N^h \end{aligned} \quad (\text{C.11})$$

In a similar way,

$$\begin{aligned} \overline{|\mathcal{M}_{N\phi}^Z| |\mathcal{M}_{N\phi}^h|^\dagger} &= \frac{1}{2} \sum_{\text{all spin}} [b_N^Z (\bar{u}_N(q_3) \gamma^\mu u_N(q_1)) (q_{2\mu} + q_{4\mu})] [\alpha_N^h (\bar{u}_N(q_3) u_N(q_1)) 1]^\dagger \\ &= \frac{b_N^Z \alpha_N^{h\dagger}}{2} \text{Tr} \left[\gamma^\mu (\not{q}_1 + m_N) (\not{q}_3 + m_N) \right] (q_{2\mu} + q_{4\mu}) \\ &= 2m_N b_N^Z \alpha_N^{h\dagger} (q_1 \cdot q_2 + q_1 \cdot q_4 + q_2 \cdot q_3 + q_3 \cdot q_4) \\ &= 2m_N b_N^Z \alpha_N^{h\dagger} 4m_\phi m_N \quad \text{as initially the nucleus is in rest, } q_1 \sim \{m_N, \vec{0}\} \\ &= 8m_N^2 m_\phi b_N^Z \alpha_N^{h\dagger} \end{aligned} \quad (\text{C.12})$$

The spin-independent pFIMP – nucleon scattering cross-section for Z mediator, taking the non-relativistic limit and assuming the initial nucleon is at rest, is given by [78],

$$\begin{aligned} \sigma_{\phi N} &= \frac{1}{4m_\phi m_N |w - v_N|} \int \frac{d^3 q_3}{(2\pi)^3 2m_N} \frac{d^3 q_4}{(2\pi)^3 2m_\phi} \overline{|\mathcal{M}_{N\phi}^Z + \mathcal{M}_{N\phi}^h|^2} (2\pi)^4 \delta^4(q_1 + q_2 - q_3 - q_4) \\ &= \int \frac{\overline{|\mathcal{M}_{N\phi}^Z + \mathcal{M}_{N\phi}^h|^2}}{4\pi^2 (4m_\phi m_N)^2 |w - v_N|} d^3 q_3 d^3 q_4 \delta(E_1 + E_2 - E_3 - E_4) \delta^3(\vec{q}_1 + \vec{q}_2 - \vec{q}_3 - \vec{q}_4) \end{aligned} \quad (\text{C.13})$$

From energy conservation,

$$\begin{aligned} 2\mu_{\phi N} \vec{q}_2 \cdot \vec{q}_3 &= m_\phi |\vec{q}_3|^2 \\ |\vec{q}_3| &= 2\mu_{\phi N} w \cos \theta \end{aligned} \quad (\text{C.14})$$

where w , v_N is the initial velocity of the dark matter and nucleus. We have assumed that in Lab-frame the nucleus initially is in rest i.e. $|\vec{v}_N| = 0$ so the relative velocity between DM and nucleus becomes w . The angle between \vec{q}_2 and \vec{q}_3 is θ . Then Eq. C.13 becomes,

$$\begin{aligned}
\sigma_{\phi N} &= \int \frac{|\mathcal{M}_{N\phi}^Z + \mathcal{M}_{N\phi}^h|^2}{4\pi^2(4m_\phi m_N)^2 w} (\pi |\vec{q}_3| d \cos \theta d|\vec{q}_3|^2) d^3 q_4 \delta(E_1 + E_2 - E_3 - E_4) \delta^3(\vec{q}_2 - \vec{q}_3 - \vec{q}_4) \\
&= \frac{|2m_N \alpha_N^h + 2m_N b_N^{Z^\dagger} 2m_\phi|^2}{4\pi(4m_\phi m_N)^2 w} \int (|\vec{q}_3| d \cos \theta d|\vec{q}_3|^2) \delta(E_1 + E_2 - E_3 - E_4) \\
&= \frac{|2m_N \alpha_N^h + 2m_N b_N^{Z^\dagger} 2m_\phi|^2}{4\pi(4m_\phi m_N)^2 w} \int (|\vec{q}_3| d \cos \theta d|\vec{q}_3|^2) \frac{1}{|\vec{q}_3| w} \delta(\cos \theta - \frac{|\vec{q}_3|}{2\mu_{\phi N} w}) \\
&= \frac{|2m_N \alpha_N^h + 2m_N b_N^{Z^\dagger} 2m_\phi|^2}{4\pi(4m_\phi m_N)^2 w^2} \int_{-1}^1 \int_0^{4\mu_{\phi N}^2 w^2} d \cos \theta d|\vec{q}_3|^2 \delta(\cos \theta - \frac{|\vec{q}_3|}{2\mu_{\phi N} w}) \\
&= \frac{|2m_N \alpha_N^h + 2m_N b_N^{Z^\dagger} 2m_\phi|^2}{4\pi(4m_\phi m_N)^2 w^2} 4\mu_{\phi N}^2 w^2 \\
&= \frac{\mu_{\phi N}^2}{4\pi m_\phi^2} \left| \alpha_N^h + 2m_\phi b_N^{Z^\dagger} \right|^2 \tag{C.15}
\end{aligned}$$

D Calculation of direct detection cross-section of WIMP

The Feynman diagrams corresponding to WIMP DM χ_1 scattering off a nucleon at tree level are shown in Fig. 7.

Higgs Mediated WIMP-Nucleon Scattering:

The two relevant interaction vertices here are $\lambda_{h\chi_1\bar{\chi}_1} h\chi_1\bar{\chi}_1$ and $\frac{m_q}{v} hq\bar{q}$. Effective Lagrangian for spin-independent direct search process can be written for higgs mediator as,

$$\mathcal{L}_{eff}^h = \frac{m_q}{v} \frac{1}{m_h^2} \lambda_{h\chi_1\bar{\chi}_1} q\bar{q}\chi_1\bar{\chi}_1 = F_q^h q\bar{q}\chi_1\bar{\chi}_1 \tag{D.1}$$

Where $\lambda_{h\chi_1\bar{\chi}_1} = -\frac{Y_1}{\sqrt{2}} \sin 2\theta$ in our model.

The matrix element for a scattering $N\chi_1 \rightarrow N\chi_1$ via higgs mediation where N stands for nucleon, is the following:

$$i\mathcal{M}_{N\chi_1}^h = \beta_N^h \left[\bar{u}_N(q_3) u_N(q_1) \right] \left[\bar{u}_{\chi_1}(q_4) u_{\chi_1}(q_2) \right] \tag{D.2}$$

where β_N^h is the DM-nucleon coupling is related with the quark level coupling F_q^h following Eq. C.3. And,

$$\begin{aligned}
|\overline{\mathcal{M}_{N\chi_1}^h}|^2 &= \frac{1}{4} \sum_{\text{all spin}} |\mathcal{M}_{N\chi_1}^h|^2 \\
&= 16m_{\chi_1}^2 m_N^2 |\beta_N^h|^2 \tag{D.3}
\end{aligned}$$

Z Mediated WIMP-Nucleon Scattering:

In the case of the Z mediator, similar to pFIMP, only vector term will contribute to SI cross-section and the effective Lagrangian,

$$\begin{aligned}
\mathcal{L}_{eff}^Z &= \frac{m_Z}{v} \frac{1}{m_Z^2} \lambda_{Z\chi_1\bar{\chi}_1} \bar{q}\gamma^\mu (c_V^q - c_A^q \gamma^5) q \bar{\chi}_1 \gamma_\mu \chi_1 && \text{SI + SD} \\
&\rightarrow \frac{m_Z}{v} \frac{c_V^q}{m_Z^2} \lambda_{Z\chi_1\bar{\chi}_1} \bar{q}\gamma^\mu q \bar{\chi}_1 \gamma_\mu \chi_1 && \text{SI} \\
&= B_q \bar{\chi}_1 \gamma^\mu \chi_1 \bar{q}\gamma_\mu q && \text{(D.4)}
\end{aligned}$$

where, $\lambda_{Z\chi_1\bar{\chi}_1} = \frac{m_Z}{v} \sin^2 \theta$.

The matrix element for a scattering $N \chi_1 \rightarrow N \chi_1$ via Z mediation is the following:

$$i\mathcal{M}_{N\chi_1}^Z = B_N^Z \left[\bar{u}_N(q_3) \gamma^\mu u_N(q_1) \right] \left[\bar{u}_{\chi_1}(q_4) \gamma_\mu u_{\chi_1}(q_2) \right] \quad \text{(D.5)}$$

where B_N^Z is the DM-nucleon coupling is related with the quark level coupling B_q is followed by the Eq. C.8. And,

$$\begin{aligned}
|\overline{\mathcal{M}_{N\chi_1}^Z}|^2 &= \frac{1}{4} \sum_{\text{all spin}} |\mathcal{M}_{N\chi_1}^Z|^2 \\
&= 16m_{\chi_1}^2 m_N^2 |B_N^Z|^2
\end{aligned} \quad \text{(D.6)}$$

Now we get the spin-independent χ_1 (WIMP) DM-nucleon scattering cross section in presence of another DM ϕ (pFIMP) as [3, 79],

$$\sigma_{\chi_1 N \text{eff}}^{\text{SI}} = \frac{\Omega_{\chi_1}}{\Omega_{\chi_1} + \Omega_\phi} \frac{\mu_{\chi_1 N}^2}{\pi} |\beta_N^h + B_N^Z|^2 \quad \text{(D.7)}$$

where $\mu_{\chi_1 N} = m_{\chi_1} m_N / (m_{\chi_1} + m_N)$ is the wimp-nucleon reduced mass, $m_N \sim 0.939$ GeV denotes the nucleon mass.

E Higgs and Z Invisible decay width

The observed (expected) upper limit on the invisible branching fraction of the Higgs boson is found to be at 95% confidence level [80, 81] with total decay width of 125.1 GeV Higgs is $3.2_{-2.2}^{+2.8}$ MeV [82],

$$\mathcal{B}_{h \rightarrow \text{invisible}} < \begin{cases} 0.145(0.103) & \text{(ATLAS)} \\ 0.18(0.10) & \text{(CMS)} \end{cases} \quad \text{(E.1)}$$

$$\Gamma_{h \rightarrow \phi\phi} = \frac{(\lambda_{\phi H} v + \mathbb{L}_h)^2}{32\pi m_h} \left(1 - 4 \frac{m_\phi^2}{m_h^2} \right)^{1/2} \Theta[m_h - 2m_\phi] \quad \text{(E.2)}$$

$$\Gamma_{h \rightarrow \chi_1 \bar{\chi}_1} = \frac{\sin^4 2\theta}{32\pi v^2} m_h (m_{\chi_1} - m_{\chi_2})^2 \left(1 - 4 \frac{m_{\chi_1}^2}{m_h^2} \right)^{3/2} \Theta[m_h - 2m_{\chi_1}] \quad \text{(E.3)}$$

The recent Z-boson Invisible decay width bound has come from various experiments like [83, 84],

$$\Gamma_{Z \rightarrow \text{invisible}} < \begin{cases} 523 \pm 16 \text{ MeV} & \text{(CMS)} \\ 503 \pm 16 \text{ MeV} & \text{(LEPComb.)} \\ 498 \pm 17 \text{ MeV} & \text{(L3)} \end{cases} \quad \text{(E.4)}$$

$$\Gamma_{Z \rightarrow \phi\phi} = \frac{\mathbb{L}_Z^2 m_Z}{16\pi} \left(1 - 4 \frac{m_\phi^2}{m_Z^2}\right)^{3/2} \Theta[m_Z - 2m_\phi] \quad (\text{E.5})$$

$$\Gamma_{Z \rightarrow \chi_1 \bar{\chi}_1} = \frac{m_Z^3 \sin^4 \theta \sin^4 \theta_w}{12\pi v^2} \left(1 + 2 \frac{m_{\chi_1}^2}{m_Z^2}\right) \left(1 - 4 \frac{m_{\chi_1}^2}{m_Z^2}\right)^{1/2} \Theta[m_Z - 2m_{\chi_1}] \quad (\text{E.6})$$

If the dark matter masses are below resonance then parameter space is also constrained by the invisible Higgs and Z decay constraints.

References

- [1] PLANCK collaboration, *Planck 2018 results. VI. Cosmological parameters*, *Astron. Astrophys.* **641** (2020) A6 [[1807.06209](#)].
- [2] P. Gondolo and G. Gelmini, *Cosmic abundances of stable particles: Improved analysis*, *Nucl. Phys. B* **360** (1991) 145.
- [3] G. Jungman, M. Kamionkowski and K. Griest, *Supersymmetric dark matter*, *Phys. Rept.* **267** (1996) 195 [[hep-ph/9506380](#)].
- [4] Y. Hochberg, E. Kuflik, T. Volansky and J.G. Wacker, *Mechanism for Thermal Relic Dark Matter of Strongly Interacting Massive Particles*, *Phys. Rev. Lett.* **113** (2014) 171301 [[1402.5143](#)].
- [5] L.J. Hall, K. Jedamzik, J. March-Russell and S.M. West, *Freeze-In Production of FIMP Dark Matter*, *JHEP* **03** (2010) 080 [[0911.1120](#)].
- [6] J. McDonald, *Thermally generated gauge singlet scalars as selfinteracting dark matter*, *Phys. Rev. Lett.* **88** (2002) 091304 [[hep-ph/0106249](#)].
- [7] M. Kaplinghat, S. Tulin and H.-B. Yu, *Direct Detection Portals for Self-interacting Dark Matter*, *Phys. Rev. D* **89** (2014) 035009 [[1310.7945](#)].
- [8] D. Pappadopulo, J.T. Ruderman and G. Trevisan, *Dark matter freeze-out in a nonrelativistic sector*, *Phys. Rev. D* **94** (2016) 035005 [[1602.04219](#)].
- [9] XENON collaboration, *Dark Matter Search Results from a One Ton-Year Exposure of XENON1T*, *Phys. Rev. Lett.* **121** (2018) 111302 [[1805.12562](#)].
- [10] XENON collaboration, *Projected WIMP sensitivity of the XENONnT dark matter experiment*, *JCAP* **11** (2020) 031 [[2007.08796](#)].
- [11] (XENON COLLABORATION)^{††}, XENON collaboration, *Search for New Physics in Electronic Recoil Data from XENONnT*, *Phys. Rev. Lett.* **129** (2022) 161805 [[2207.11330](#)].
- [12] PANDAX-II collaboration, *Search for Light Dark Matter-Electron Scatterings in the PandaX-II Experiment*, *Phys. Rev. Lett.* **126** (2021) 211803 [[2101.07479](#)].
- [13] PANDAX-4T collaboration, *Dark Matter Search Results from the PandaX-4T Commissioning Run*, *Phys. Rev. Lett.* **127** (2021) 261802 [[2107.13438](#)].
- [14] LZ collaboration, *First Dark Matter Search Results from the LUX-ZEPLIN (LZ) Experiment*, [2207.03764](#).
- [15] J. Goodman, M. Ibe, A. Rajaraman, W. Shepherd, T.M.P. Tait and H.-B. Yu, *Constraints on Light Majorana dark Matter from Colliders*, *Phys. Lett. B* **695** (2011) 185 [[1005.1286](#)].
- [16] J. Goodman, M. Ibe, A. Rajaraman, W. Shepherd, T.M.P. Tait and H.-B. Yu, *Constraints on Dark Matter from Colliders*, *Phys. Rev. D* **82** (2010) 116010 [[1008.1783](#)].
- [17] A. Rajaraman, W. Shepherd, T.M.P. Tait and A.M. Wijangco, *LHC Bounds on Interactions of Dark Matter*, *Phys. Rev. D* **84** (2011) 095013 [[1108.1196](#)].
- [18] P.J. Fox, R. Harnik, J. Kopp and Y. Tsai, *Missing Energy Signatures of Dark Matter at the LHC*, *Phys. Rev. D* **85** (2012) 056011 [[1109.4398](#)].
- [19] O. Buchmueller, M.J. Dolan and C. McCabe, *Beyond Effective Field Theory for Dark Matter Searches at the LHC*, *JHEP* **01** (2014) 025 [[1308.6799](#)].

- [20] A.A. Petrov and W. Shepherd, *Searching for dark matter at LHC with Mono-Higgs production*, *Phys. Lett. B* **730** (2014) 178 [[1311.1511](#)].
- [21] W. Altmannshofer, P.J. Fox, R. Harnik, G.D. Kribs and N. Raj, *Dark Matter Signals in Dilepton Production at Hadron Colliders*, *Phys. Rev. D* **91** (2015) 115006 [[1411.6743](#)].
- [22] R.M. Capdevilla, A. Delgado, A. Martin and N. Raj, *Characterizing dark matter at the LHC in Drell-Yan events*, *Phys. Rev. D* **97** (2018) 035016 [[1709.00439](#)].
- [23] N.F. Bell, Y. Cai, J.B. Dent, R.K. Leane and T.J. Weiler, *Dark matter at the LHC: Effective field theories and gauge invariance*, *Phys. Rev. D* **92** (2015) 053008 [[1503.07874](#)].
- [24] Z.-H. Yu, Q.-S. Yan and P.-F. Yin, *Detecting interactions between dark matter and photons at high energy e^+e^- colliders*, *Phys. Rev. D* **88** (2013) 075015 [[1307.5740](#)].
- [25] R. Essig, J. Mardon, M. Papucci, T. Volansky and Y.-M. Zhong, *Constraining Light Dark Matter with Low-Energy e^+e^- Colliders*, *JHEP* **11** (2013) 167 [[1309.5084](#)].
- [26] K. Kadota and J. Silk, *Constraints on Light Magnetic Dipole Dark Matter from the ILC and SN 1987A*, *Phys. Rev. D* **89** (2014) 103528 [[1402.7295](#)].
- [27] Z.-H. Yu, X.-J. Bi, Q.-S. Yan and P.-F. Yin, *Dark matter searches in the mono-Z channel at high energy e^+e^- colliders*, *Phys. Rev. D* **90** (2014) 055010 [[1404.6990](#)].
- [28] A. Freitas and S. Westhoff, *Leptophilic Dark Matter in Lepton Interactions at LEP and ILC*, *JHEP* **10** (2014) 116 [[1408.1959](#)].
- [29] S. Dutta, D. Sachdeva and B. Rawat, *Signals of Leptophilic Dark Matter at the ILC*, *Eur. Phys. J. C* **77** (2017) 639 [[1704.03994](#)].
- [30] M. Habermehl, M. Berggren and J. List, *WIMP Dark Matter at the International Linear Collider*, *Phys. Rev. D* **101** (2020) 075053 [[2001.03011](#)].
- [31] E.A. Baltz, M. Battaglia, M.E. Peskin and T. Wizansky, *Determination of dark matter properties at high-energy colliders*, *Phys. Rev. D* **74** (2006) 103521 [[hep-ph/0602187](#)].
- [32] G. Bélanger et al., *LHC-friendly minimal freeze-in models*, *JHEP* **02** (2019) 186 [[1811.05478](#)].
- [33] C. Boehm, D. Hooper, J. Silk, M. Casse and J. Paul, *MeV dark matter: Has it been detected?*, *Phys. Rev. Lett.* **92** (2004) 101301 [[astro-ph/0309686](#)].
- [34] C. Boehm, T.A. Ensslin and J. Silk, *Can Annihilating dark matter be lighter than a few GeVs?*, *J. Phys. G* **30** (2004) 279 [[astro-ph/0208458](#)].
- [35] A.J. Tylka and F.W. Stecker, γ^- ray SIGNATURES OF DARK MATTER ANNIHILATION IN THE GALAXY, 6, 1989.
- [36] S. Stephens, *Antiprotons in cosmic rays and their implications*, *Advances in Space Research* **9** (1989) 55.
- [37] C.S. Shen and G.B. Berkey, *Antiprotons and positrons in cosmic rays*, *Phys. Rev.* **171** (1968) 1344.
- [38] F.W. Stecker and A.J. Tylka, *Cosmic-ray antiproton spectrum from dark matter annihilation and its astrophysical implications - a new look*, *Astrophys. J.; (United States)* .
- [39] C. Evoli, I. Cholis, D. Grasso, L. Maccione and P. Ullio, *Antiprotons from dark matter annihilation in the Galaxy: astrophysical uncertainties*, *Phys. Rev. D* **85** (2012) 123511 [[1108.0664](#)].

- [40] T. Delahaye, R. Lineros, F. Donato, N. Fornengo and P. Salati, *Positrons from dark matter annihilation in the galactic halo: Theoretical uncertainties*, *Phys. Rev. D* **77** (2008) 063527 [[0712.2312](#)].
- [41] L. Bergstrom, T. Bringmann, I. Cholis, D. Hooper and C. Weniger, *New Limits on Dark Matter Annihilation from AMS Cosmic Ray Positron Data*, *Phys. Rev. Lett.* **111** (2013) 171101 [[1306.3983](#)].
- [42] A.J. Tylka, *Cosmic Ray Positrons From Annihilation of Weakly Interacting Massive Particles in the Galaxy*, *Phys. Rev. Lett.* **63** (1989) 840.
- [43] Q.-H. Cao, E. Ma, J. Wudka and C.P. Yuan, *Multipartite dark matter*, [0711.3881](#).
- [44] K.M. Zurek, *Multi-Component Dark Matter*, *Phys. Rev. D* **79** (2009) 115002 [[0811.4429](#)].
- [45] S. Profumo, K. Sigurdson and L. Ubaldi, *Can we discover multi-component WIMP dark matter?*, *JCAP* **12** (2009) 016 [[0907.4374](#)].
- [46] S. Bhattacharya, A. Drozd, B. Grzadkowski and J. Wudka, *Two-Component Dark Matter*, *JHEP* **10** (2013) 158 [[1309.2986](#)].
- [47] B. Díaz Sáez, K. Möhling and D. Stöckinger, *Two real scalar WIMP model in the assisted freeze-out scenario*, *JCAP* **10** (2021) 027 [[2103.17064](#)].
- [48] G. Belanger and J.-C. Park, *Assisted freeze-out*, *JCAP* **03** (2012) 038 [[1112.4491](#)].
- [49] T.N. Maity and T.S. Ray, *Exchange driven freeze out of dark matter*, *Phys. Rev. D* **101** (2020) 103013 [[1908.10343](#)].
- [50] P. Ghosh, P. Konar, A.K. Saha and S. Show, *Self-interacting freeze-in dark matter in a singlet doublet scenario*, *JCAP* **10** (2022) 017 [[2112.09057](#)].
- [51] S. Bhattacharya, J. Lahiri and D. Pradhan, *Dynamics of the pseudo-FIMP in presence of a thermal Dark Matter*, [2212.07622](#).
- [52] F. del Aguila, L. Ametller, G.L. Kane and J. Vidal, *Vector Like Fermion and Standard Higgs Production at Hadron Colliders*, *Nucl. Phys. B* **334** (1990) 1.
- [53] CMS collaboration, *Search for invisible decays of a Higgs boson produced through vector boson fusion in proton-proton collisions at $\sqrt{s} = 13$ TeV*, *Phys. Lett. B* **793** (2019) 520 [[1809.05937](#)].
- [54] K. Griest and D. Seckel, *Three exceptions in the calculation of relic abundances*, *Phys. Rev. D* **43** (1991) 3191.
- [55] R.T. D’Agnolo, D. Pappadopulo and J.T. Ruderman, *Fourth exception in the calculation of relic abundances*, *Phys. Rev. Lett.* **119** (2017) 061102.
- [56] G. Bélanger, F. Boudjema, A. Pukhov and A. Semenov, *micrOMEGAs4.1: two dark matter candidates*, *Comput. Phys. Commun.* **192** (2015) 322 [[1407.6129](#)].
- [57] R.T. D’Agnolo, C. Mondino, J.T. Ruderman and P.-J. Wang, *Exponentially Light Dark Matter from Coannihilation*, *JHEP* **08** (2018) 079 [[1803.02901](#)].
- [58] C.-K. Chua and R.-C. Hsieh, *Study of Dirac fermionic dark matter*, *Phys. Rev. D* **88** (2013) 036011 [[1305.7008](#)].
- [59] J. Edsjo and P. Gondolo, *Neutralino relic density including coannihilations*, *Phys. Rev. D* **56** (1997) 1879 [[hep-ph/9704361](#)].

- [60] G. Duda, G. Gelmini, P. Gondolo, J. Edsjo and J. Silk, *Indirect detection of a subdominant density component of cold dark matter*, *Phys. Rev. D* **67** (2003) 023505 [[hep-ph/0209266](#)].
- [61] P. Ullio, L. Bergstrom, J. Edsjo and C.G. Lacey, *Cosmological dark matter annihilations into gamma-rays - a closer look*, *Phys. Rev. D* **66** (2002) 123502 [[astro-ph/0207125](#)].
- [62] V. Gammaldi, J. Pérez-Romero, J. Coronado-Blázquez, M. Di Mauro, E.V. Karukes, M.A. Sánchez-Conde et al., *Dark matter search in dwarf irregular galaxies with the fermi large area telescope*, *Phys. Rev. D* **104** (2021) 083026.
- [63] SUPER-KAMIOKANDE collaboration, *Indirect search for dark matter from the Galactic Center and halo with the Super-Kamiokande detector*, *Phys. Rev. D* **102** (2020) 072002 [[2005.05109](#)].
- [64] H.E.S.S. collaboration, *Search for Dark Matter Annihilation Signals in the H.E.S.S. Inner Galaxy Survey*, *Phys. Rev. Lett.* **129** (2022) 111101 [[2207.10471](#)].
- [65] ICECUBE collaboration, *Observation and Characterization of a Cosmic Muon Neutrino Flux from the Northern Hemisphere using six years of IceCube data*, *Astrophys. J.* **833** (2016) 3 [[1607.08006](#)].
- [66] ICECUBE collaboration, *Searches for Connections between Dark Matter and High-Energy Neutrinos with IceCube*, [2205.12950](#).
- [67] ICECUBE collaboration, *Search for GeV-scale dark matter annihilation in the Sun with IceCube DeepCore*, *Phys. Rev. D* **105** (2022) 062004 [[2111.09970](#)].
- [68] B. Díaz Sáez, P. Escalona, S. Norero and A.R. Zerwekh, *Fermion singlet dark matter in a pseudoscalar dark matter portal*, *JHEP* **10** (2021) 233 [[2105.04255](#)].
- [69] A. Reinert and M.W. Winkler, *A Precision Search for WIMPs with Charged Cosmic Rays*, *JCAP* **01** (2018) 055 [[1712.00002](#)].
- [70] FERMI-LAT collaboration, *Searching for Dark Matter Annihilation from Milky Way Dwarf Spheroidal Galaxies with Six Years of Fermi Large Area Telescope Data*, *Phys. Rev. Lett.* **115** (2015) 231301 [[1503.02641](#)].
- [71] M.D. Schwartz, *Quantum Field Theory and the Standard Model*, Cambridge University Press (3, 2014).
- [72] M.E. Peskin and D.V. Schroeder, *An Introduction to quantum field theory*, Addison-Wesley, Reading, USA (1995).
- [73] H.H. Patel, *Package-X 2.0: A Mathematica package for the analytic calculation of one-loop integrals*, *Comput. Phys. Commun.* **218** (2017) 66 [[1612.00009](#)].
- [74] V. Shtabovenko, R. Mertig and F. Orellana, *FeynCalc 9.3: New features and improvements*, *Comput. Phys. Commun.* **256** (2020) 107478 [[2001.04407](#)].
- [75] G. Bertone, D. Hooper and J. Silk, *Particle dark matter: Evidence, candidates and constraints*, *Phys. Rept.* **405** (2005) 279 [[hep-ph/0404175](#)].
- [76] J. Ellis, N. Nagata and K.A. Olive, *Uncertainties in WIMP Dark Matter Scattering Revisited*, *Eur. Phys. J. C* **78** (2018) 569 [[1805.09795](#)].
- [77] P. Agrawal, Z. Chacko, C. Kilic and R.K. Mishra, *A Classification of Dark Matter Candidates with Primarily Spin-Dependent Interactions with Matter*, [1003.1912](#).
- [78] T. Lin, *Dark matter models and direct detection*, *PoS* **333** (2019) 009 [[1904.07915](#)].

- [79] J. Hisano, R. Nagai and N. Nagata, *Effective Theories for Dark Matter Nucleon Scattering*, *JHEP* **05** (2015) 037 [[1502.02244](#)].
- [80] ATLAS collaboration, *Search for invisible Higgs-boson decays in events with vector-boson fusion signatures using 139 fb⁻¹ of proton-proton data recorded by the ATLAS experiment*, *JHEP* **08** (2022) 104 [[2202.07953](#)].
- [81] CMS collaboration, *Search for invisible decays of the Higgs boson produced via vector boson fusion in proton-proton collisions at s=13 TeV*, *Phys. Rev. D* **105** (2022) 092007 [[2201.11585](#)].
- [82] PARTICLE DATA GROUP collaboration, *Review of Particle Physics*, *PTEP* **2022** (2022) 083C01.
- [83] CMS collaboration, *Precision measurement of the Z invisible width with the CMS experiment in pp collisions at $\sqrt{s} = 13$ TeV*, .
- [84] CMS collaboration, *Precision measurement of the Z boson invisible width in pp collisions at $\sqrt{s} = 13$ TeV*, [2206.07110](#).